The Astronomical Journal, 128:2144–2169, 2004 November

ON DETERMINING EXTINCTION FROM REDDENING[1]

Marshall L. McCall
Department of Physics and Astronomy, 4700 Keele Street, Toronto, ON M3J 1P3, Canada; mccall@yorku.ca
Received 2002 August 7; accepted 2004 August 4

ABSTRACT

The influence of shifts in effective wavelengths on ratios of total to selective extinction is examined, primarily to determine how to evaluate the Galactic extinction of extragalactic bodies in a way that minimizes systematic errors. In the process, a new procedure is developed for evaluating the Galactic or extragalactic extinction of any source in any filter from any index of reddening. The amount of dust along a sightline is quantified by the optical depth at 1 μm, which has the advantage of being roughly equal numerically to $E(B-V)$. The optical depth can be derived iteratively from a color excess using an appropriate spectral energy distribution (SED) for the reddening probe, and a monochromatic law of reddening which delivers a value of $A_V/E(B-V)$ characteristic of the obscuring medium when applied to the spectrum of a reference source for which this ratio is known. Knowledge of the optical depth then facilitates the determination of the extinction of any source in any filter without concern as to the shape of the spectrum of the probe. The ratio of total to selective extinction for stars and galaxies is synthesized for a variety of filter combinations in order to examine variations with type, tilt, optical depth, and redshift. For this purpose, representative *integrated* SEDs spanning the space ultraviolet to the near-infrared are constructed for galaxy types E, Sab, Sbc, Scd, and Im, all at well-defined inclinations. In addition, an algorithm to adjust the shapes of the SEDs for tilt is developed. Along the main sequence, the classical ratio of total to selective extinction, $A_V/E(B-V)$, increases by 23% from O5 to M6. At late types, there are differences as high as 17% between evolved and unevolved stars. Along the Hubble sequence, $A_V/E(B-V)$ decreases by 5% from E to Im. The value for elliptical galaxies falls near the locus for the main sequence, not the giant branch. Correlated against $B-I$, $A_V/E(B-V)$ for star-forming galaxies is systematically lower than for stars of the same color by up to 5%. It increases much more rapidly with tilt than with the optical depth of Galactic dust, although neither dependence is strong. For both stars and galaxies, $A_V/E(B-V)$ varies dramatically with the redshift. Changes of 16% for a Type Ia supernovae and 22% for a Cepheid are seen out to $z = 0.4$. For elliptical galaxies, a variation of 30% can be expected out to $z = 1$, the precise form of which being dependent upon the ultraviolet excess. Even infrared ratios of total to selective extinction, such as $A_H/E(B-V)$, change significantly with color and redshift because of differential shifts in the effective wavelengths of B and V. As a gauge of reddening, $E(V-I)$ is greatly preferable to $E(B-V)$, because it is much less sensitive to color and redshift, yet more sensitive to the optical depth of dust. A demonstration is given on how to quantify upper limits to Galactic extinction which should be placed on studies of high-redshift supernovae, to reduce the redshift dependence of extinction corrections to a range that is insignificant compared with residuals supporting accelerated universal expansion. When the new technique for evaluating extinction corrections is applied to Cepheids in M31, distances for fields at different radii become less dispersed, confirming that the period-luminosity relation is not very sensitive to metallicity. However, the discrepancy between the Cepheid and maser distances to NGC 4258 cannot be attributed to the method of handling the extinction.

Key words: Cepheids — dust, extinction — galaxies: general — stars: general — supernovae: general — techniques: photometric

1. INTRODUCTION

There are many ways of precisely measuring the reddening of a celestial body or its constituents, because it is easy to judge the unobscured color, say, through examination of counterparts at high Galactic latitude. For example, Burstein & Heiles (1982) calibrated $E(B-V)$ toward extragalactic sources using $B-V$ colors of field RR Lyrae stars and stars in globular clusters, while Schlegel et al. (1998) used the relationship between the Mg_2 index and intrinsic $B-V$ color for elliptical galaxies. However, few methods are available for directly evaluating the extinction, especially of extragalactic sources, and they are not very accurate (McCall & Armour 2000). This is because it is normally impossible to know the unobscured magnitude of a source, owing to its linkage to the distance. Fortunately, extinction correlates with reddening. In principle, then, the extinction of a source can be derived from a measurement of the reddening. The hitch is that the "constant" of proportionality connecting the two, better known as the *the ratio of total to selective extinction*, is not constant. Yet, very often, distances and intrinsic properties of sources are founded upon an assumption that it is. Resulting errors are *systematic* and grow with the level of obscuration.

Traditionally, the ratio of total to selective extinction, normally designated by R, has been defined as the constant of proportionality connecting the total extinction in V, A_V, to the difference in extinction between B and V, $E(B-V) = A_B - A_V$. Symbolically,

$$R = A_V/E(B-V). \quad (1)$$

[1] Submission of the final version of this paper was held off until the techniques described herein could be made available through the World Wide Web. The York Extinction Solver (YES) can be accessed at http://cadcwww.hia.nrc.ca/yes.

The quantity $E(B-V)$ is referred to as the *reddening* or *color excess* because it is derived from the difference between the apparent color $B-V$ and the unobscured color $(B-V)^0$.

The extinction in any bandpass correlates with the color excess determined from any pair of bandpasses. Equation (1) can be generalized for an arbitrary filter Λ as follows:

$$R_\Lambda = A_\Lambda / E(B-V). \tag{2}$$

As a consequence, it is appropriate to replace R in equation (1) with R_V if $\Lambda = V$.

Underlying the relationship between the extinction and color excess is a *reddening law*, which determines how the monochromatic extinction A_λ varies with wavelength λ. Normally, the reddening law is described by *extinction coefficients* R_λ defined as follows:

$$R_\lambda = A_\lambda / E(B-V). \tag{3}$$

The normalization of A_λ to $E(B-V)$ is in place to make the law scale-free, that is, to make it representative of the average properties of dust along a line of sight, but independent of the actual quantity of dust that is there. Most measurements of R_λ come from broadband photometry and/or spectroscopy of O and B stars.

How R_λ varies with wavelength, and to a large extent the values of R_Λ, are determined by the nature of interstellar dust. For example, in all directions in the Milky Way, R_λ increases toward the ultraviolet. This is a result of the grain size distribution, which favors small particles over large ones. For the diffuse component of the interstellar medium, which is responsible for extinction along most lines of sight, dust and the reddening law imposed by it are referred to as "normal." The value of R_V is around 3. However, R_V approaches 6 toward the cores of dense molecular clouds and regions where there has been recent star formation, such as in the Orion Nebula. Such variations are believed to be due to changes in the grain size distribution, as can arise from preferential evaporation of small grains or accretion (see, e.g., McCall 1981).

The overall shape of the reddening law appears to be determined by one parameter (Cardelli et al. 1989), henceforth designated by r. Thus,

$$R_\lambda = \phi(r). \tag{4}$$

A good choice for r is R_V (Cardelli et al. 1989). However, there are changes in fine structure, primarily the position and width of the "bump" in extinction located at 2200 Å, that do not correlate with R_V. Random variations in the chemical composition of the grains, or at least the mix of grain types, are probably responsible.

Unfortunately, R_Λ also depends upon the measurement process. This is because a detector sees a spectral energy distribution (SED) weighted by a system response function, the latter determined primarily by the transmission curve of the filter. This affects not only A_Λ, but also $E(B-V)$. Typically, a filter used to study a galaxy (such as B or V) is very broad, so the flux-weighted wavelength of detected photons, referred to as the *effective wavelength*, can vary with the shape of the SED; it depends upon how the light of the source is distributed across the bandpass. Therefore, at a given reddening, the extinction affecting a measured magnitude, even after transformations take out color terms, depends upon the SED. Even if dust were the same everywhere, R_Λ would vary from source to source. Even R_λ, the so called monochromatic reddening law, contains, through its normalization to $E(B-V)$, a distinctly nonmonochromatic component tied to the sources used to measure it. In addition, the wavelengths at which values of R_λ are specified may be effective wavelengths for broadband filters and therefore tied to the SEDs of the objects used to measure the coefficents.

For stars, it has long been known that $R_V = A_V/E(B-V)$ depends upon both intrinsic color and the amount of reddening (see, e.g., Blanco 1956; Schmidt 1956; Olson 1975). There may also be some sensitivity to metallicity, because Racine (1973) found that for globular clusters $E(U-B)/E(B-V)$ varies with integrated spectral type. For stars in the Milky Way obscured by normal dust, Schmidt-Kaler (1982) advocates

$$R_V = R_V^{00} + 0.28(B-V)^0 + 0.04E(B-V), \tag{5}$$

where $(B-V)^0$ is the intrinsic color, $E(B-V)$ is the reddening, and R_V^{00} is the ratio of total to selective extinction for a star of zero color in the limit of zero reddening. For a given layer of dust, an intrinsically redder star *appears* to suffer more extinction per unit reddening. The explanation lies in the effective wavelengths. They are redder for both B and V, but the extinction in B is reduced more than in V. Thus, $E(B-V)$ is lowered with respect to A_V, and R_V is increased.

Today, reddenings of celestial bodies are defined by myriads of filter combinations, and they may be called upon to evaluate extinction in a wide variety of bandpasses. Outside of U, B, and V, very little research has been done to define how the corresponding ratios of total to selective extinction depend upon SEDs. In fact, no research has been done to judge how the ratio of total to selective extinction might vary from galaxy to galaxy, and only one study has ever been performed to determine what the appropriate value might be for *any* galaxy (Schlegel et al. 1998, for elliptical galaxies only). As a result, the derivation of the extinction of a galaxy may be filled with inconsistencies. Using the NASA/IPAC Extragalactic Database (NED),[2] a researcher could arrive at an extinction for a *spiral galaxy* that is founded upon a color index for *elliptical galaxies* (Schlegel et al. 1998) and a reddening law for *O and B stars* (Cardelli et al. 1989)!

Of particular concern is that galaxies and their constituents can have radial velocities much greater than those of stars in the Milky Way. No study has ever been made for galaxies to determine how motions affect ratios of total to selective extinction. The only kinds of stars for which any kind of study has been performed is Type Ia supernovae (Nugent et al. 2002). It is shown in this paper that R_V, especially, is very sensitive to the velocity of the source. The SED of a galaxy or star at a redshift of 0.05 (velocity 15,000 km s^{-1}) is shifted 12% of the way across the B band. For an Sbc galaxy, R_V rises from 3.08 to 3.15. For a G8 supergiant (a long-period Cepheid), it increases from 3.39 to 3.60.

In this paper, the ratio of total to selective extinction for stars and galaxies is studied, with the objective of developing a system for evaluating the extinction of any source in any bandpass in a manner that accounts properly for the intrinsic shape of the spectrum, obscuration by dust in the frame of the source, the redshift, and obscuration by dust in the Milky Way.

[2] The NASA/IPAC Extragalactic Database (NED) is operated by the Jet Propulsion Laboratory, California Institute of Technology, under contract with NASA.

The work is motivated by the need for reliable extinction estimates for extragalactic sources obscured predominantly by dust in the diffuse component of the interstellar medium. In § 2, problems with current practices of correcting for extinction are described, and the relevance of R_Λ to various realms of research is discussed. In § 3, a new way of quantifying the extinction of a source is developed, and the ingredients required to estimate R_Λ for any object, namely, the reddening law, filter response functions, and integrated SEDs, are gathered. In § 4, the ingredients are pooled to examine how R_Λ varies with the shape of the SED, extinction, and redshift, both in the optical and the near-infrared. Recommendations on how to determine the Galactic extinction of *any* source in *any* bandpass are given in § 5. Two examples involving extragalactic Cepheid variables are presented as well. Conclusions are presented in § 6.

2. CURRENT ISSUES

Many extragalactic astronomers draw upon extinction corrections advertised by the Third Reference Catalogue of Bright Galaxies (RC3; de Vaucouleurs et al. 1991) or by NED. However, these corrections are intrinsically flawed. Burstein & Heiles (1984) and the RC3 both employ the maps of $E(B-V)$ by Burstein & Heiles (1982) to estimate A_B for galaxies. Burstein & Heiles (1984) fix R_V at 3.0 for all galaxies, which is a value appropriate for O and B stars, but the RC3 fixes R_V at 3.3, a value derived for stars with the same color as an average galaxy. In NED, extinction estimates from the maps of Burstein & Heiles (1982) are derived using $R_V = 3.0$ [actually, $A_B = 4.0E(B-V) + 0.005$: H. G. Corwin 2002, private communication], but values from the maps of Schlegel et al. (1998) are derived using $R_V = 3.315$, which is the value Schlegel et al. (1998) computed for an unobscured elliptical galaxy at rest using the "$R_V = 3.1$" reddening law of Cardelli et al. (1989). All of these choices are linked in one way or another to reddening laws founded upon broadband photometry of O and B stars.

Another problem facing modern astronomers is how to evaluate the extinction in a bandpass different from one for which the extinction is already known. For example, a researcher working in H typically will derive a value for A_H from A_V on the basis of a reddening law defining A_H/A_V. The wrong answer for A_H would result because A_H/A_V is not a constant. How A_H varies with the source spectrum, the reddening, and the redshift differs from the way A_V does.

To put all of this into perspective, it is worth looking at a few instances of where the ratio of total to selective extinction has a bearing on our understanding of the extragalactic universe:

Distances and absolute magnitudes of galaxies.—Usually, the best estimates of the distance of a galaxy come from photometry of stellar constituents. However, all must be corrected for extinction. The extinction is usually gauged from a color excess with the aid of a reddening law. However, sources used to measure the color excess, the reddening law, and the distance are usually all different. Since R_Λ varies drastically with spectral type and luminosity class, failure to account for these differences will inevitably lead to an errant distance. If the extinction is large enough, the failure may be evidenced by disagreements among different distance indicators, or by residuals that vary with redshift. Photometry of the galaxy itself also must be corrected for reddening to arrive at an absolute magnitude. The wrong answer could follow if a value of R_Λ used for stellar constituents were applied to the galaxy as a whole.

Surface brightness profiles of galaxies.—R_Λ may vary across the face of a galaxy displaying a color gradient. The extinction correction for the bulge in a spiral ought to be different from that for the disk.

Galaxian luminosity functions.—Even if the optical depth of Galactic dust across the face of a cluster is uniform, different values of R_Λ ought to be adopted to correct magnitudes of different kinds of galaxies for extinction, owing to the different shapes of their spectra. The problem is particularly acute in studies of the luminosity function of nearby galaxies, which by necessity must include objects in the Zone of Avoidance. It is also relevant to research into the Great Attractor, the constituents of which are heavily obscured (Woudt & Kraan-Korteweg 2000).

Bulk flows.—Characteristics of large-scale flows are derived using samples of galaxies spread over a wide area of sky and spanning a large range of redshift. Errors in flow parameters could arise if significant systematic errors in relative distances are present, as could be the case if R_Λ varies enough with reddening and/or redshift. Any error in R_Λ propagates into an error in A_Λ that grows with A_Λ. Consequently, how R_Λ varies from galaxy to galaxy may be important even if the extinction is relatively low.

Population syntheses.—Insights into the evolutionary state of multicomponent systems can be gained by synthesizing integrated spectra. The shape of the continuum can be an important constraint. For example, in modeling early-type galaxies, the continuum plays a role in defining the mix of stellar populations (Pickles 1985). At first glance, it might seem that spectroscopy is immune to the kinds of problems inherent in the correction of broadband photometry for extinction. However, invariably a broadband index of reddening has to be used to determine the size of the extinction correction at every wavelength. As a result, even though extinction corrections are monochromatic, their precise values depend upon, through R_λ, the spectrum of the probe of reddening and the kinds of targets used to define the reddening law.

More quantitatively, consider Maffei 1, the nearest giant elliptical galaxy. Based upon its Mg_2 index, $E(B-V)$ is 1.56 (Fingerhut et al. 2003). Blindly adopting $R_V = 3.1$, then $A_V = 4.8$. Guided by equation (5), however, $R_V = 3.4$ (if $R_V^{00} = 3.1$), and $A_V = 5.3$. The difference, fully half a magnitude in V, translates into a distance error of 20% if the velocity dispersion is used to gauge the absolute magnitude. In the near-infrared, say, H, the extinction is reduced, but it is not zero. Typically, the optical result would be used to derive it. A reddening law might indicate that $A_H/A_V = 0.19$ (Cardelli et al. 1989). Which estimate of A_V, if any, should be used to work out A_H?

Now consider Maffei 2, a nearby Sbc spiral close in the sky to Maffei 1. The flux ratio $F(\mathrm{H}\alpha)/F(\mathrm{H}\beta)$ observed for embedded H II regions can be used to quantify the amount of reddening (see McCall 1989). A reddening law gives $A_\lambda/E(B-V)$ at each wavelength, permitting computation of $E(B-V)$. The reddening estimated this way is greater than for Maffei 1 (Fingerhut 2002). However, Maffei 2 is bluer than Maffei 1. Is A_V greater?

3. METHOD

3.1. *Broadband Extinction*

The extinction of a source is determined by how much the observed flux is suppressed relative to what it would be if there were no dust along the line of sight. For a

broadband filter, the observed flux is determined by the following:

1. The spectrum of redshifted flux from the source per unit wavelength, $F_\lambda(z)$, that arrives at the Milky Way;

2. The monochromatic extinction, A_λ, as a function of wavelength due to dust in the Milky Way; and

3. The transmission, $T_\lambda(\Lambda)$, as a function of wavelength (usually called the *response function*) of the particular observing system (atmosphere, telescope, filter, instrument, and detector).

It is quantified by the *effective flux* per unit wavelength, $F_{\lambda,\,\mathrm{eff}}$, which is defined by

$$F_{\lambda,\,\mathrm{eff}}(\Lambda) = \frac{\int_0^\infty D(\lambda)T_\lambda(\Lambda)F_\lambda(z)10^{-A_\lambda/2.5}\,d\lambda}{\int_0^\infty D(\lambda)T_\lambda(\Lambda)d\lambda}, \tag{6}$$

where $D(\lambda)$ is a function that depends upon the characteristics of the photometric system, that is, how T_λ is defined.

Despite what instrumentation is used to actually make observations, transformation equations lead to magnitudes determined by the equipment originally used to define the photometric system. If that equipment employed a detector whose sensitivity was characterized by the efficiency of current generation, such as would be the case for a photoelectric tube, then $D(\lambda) = 1$. If the equipment employed a detector characterized in terms of the efficiency of counting photons, such as a CCD, then $D(\lambda) = \lambda$.

The perceived extinction through filter Λ is given by

$$A_\Lambda = -2.5\log F_{\lambda,\,\mathrm{eff}}(\Lambda)/F^0_{\lambda,\,\mathrm{eff}}(\Lambda), \tag{7}$$

where $F^0_{\lambda,\,\mathrm{eff}}$ is the effective flux that would be seen if there were no Galactic dust along the line of sight. Thus, A_Λ, and, in turn, R_Λ, depends upon the intrinsic SED (F_λ for $z = 0$), z, and the optical depth of the interstellar medium. This is because the flux-weighted mean wavelength of a bandpass shifts with changes in the shape of the *apparent* SED. A useful approximation to this mean is the *effective wavelength*, defined by

$$\lambda_{\mathrm{eff}}(\Lambda) = \frac{\int_0^\infty \lambda D(\lambda)T_\lambda(\Lambda)F_\lambda(z)10^{-A_\lambda/2.5}\,d\lambda}{\int_0^\infty D(\lambda)T_\lambda(\Lambda)F_\lambda(z)10^{-A_\lambda/2.5}\,d\lambda}. \tag{8}$$

For a source with a smooth spectrum, the effective flux is very close to the monochromatic flux in the apparent SED at the effective wavelength (Golay 1974).

3.2. *Monochromatic Extinction*

Based upon equations (3) and (4), the monochromatic extinction A^{src}_λ of a source is related to its reddening $E(B-V)^{\mathrm{src}}$ as follows:

$$A^{\mathrm{src}}_\lambda = R_\lambda(r)E(B-V)^{\mathrm{src}}. \tag{9}$$

What makes this different from equation (3) is that R_λ is not usually defined by A^{src}_λ and $E(B-V)^{\mathrm{src}}$, but rather by a reddening law derived from analyses of *different* objects. The problem is that both $E(B-V)^{\mathrm{src}}$ and R_λ depend upon broadband measures of extinction. To use equation (9) correctly, it is necessary to renormalize the reddening law to the same $E(B-V)$ as that indexing the extinction of the source. This requires knowledge of the relation between $E(B-V)$ for objects defining the reddening law and for objects defining $E(B-V)$ for the source. Clearly, the task is difficult, and almost never done.

Equation (9) is logically flawed, in that it links an effect of obscuration by a layer of dust to another effect of that obscuration. What is needed is a linkage between the effect and its cause, which is optical depth. This can be accomplished by normalizing the extinction coefficients to the optical depth at some reference wavelength if the numerators are truly monochromatic. Denoting the optical depth of the source at wavelength λ by $\tau^{\mathrm{src}}_\lambda$ and the reference wavelength by λ_{ref},

$$A^{\mathrm{src}}_\lambda = (2.5\log e)[R_\lambda(r)/R_{\lambda_{\mathrm{ref}}}(r)]\tau^{\mathrm{src}}_{\lambda_{\mathrm{ref}}}. \tag{10}$$

An excellent choice for the reference wavelength is 1 μm. In the near-infrared, R_λ is not very sensitive to environment (Cardelli et al. 1989). In fact, for this reason, Binney & Merrifield (1998) advocate normalizing reddening laws to a bandpass redward of V, although they do not recognize the significance of effective wavelength shifts. For bluish sources at low redshift, the optical depth at 1 μm is numerically only about 10% larger than $E(B-V)$ (see Fig. 8), which is convenient for mental evaluation of the observational implications of a particular value. Setting λ_{ref} to 1 μm, then

$$A^{\mathrm{src}}_\lambda = R'_\lambda(r)\tau^{\mathrm{src}}_1, \tag{11}$$

where τ^{src}_1 is the optical depth toward the source at 1 μm. The revised extinction coefficient, R'_λ, is defined by

$$\begin{aligned} R'_\lambda(r) &= (2.5\log e)\frac{R_\lambda(r)}{R_1(r)}, \\ &= A_\lambda/\tau_1, \end{aligned} \tag{12}$$

where R_1 is R_λ at 1 μm.

If r is defined appropriately (see below), substitution of equation (11) into equation (6) leads to an expression for the extinction A_Λ (eq. [7]) perceived through a filter that does not depend upon the kinds of sources used to define the reddening law. Then, it becomes possible to define a ratio of total to selective extinction for the filter that does not depend upon the characteristics of any other filter, namely,

$$R'_\Lambda(r) = A_\Lambda/\tau_1. \tag{13}$$

Equations (6), (7), (11), and (12) form the foundation for investigating how R'_Λ (eq. [13]), and, in turn, R_Λ (eq. [2]), depend upon the intrinsic spectrum of a source, obscuration by associated dust, redshift, and Galactic extinction. However, before they can be used, it is necessary to identify the appropriate reddening law, response functions, and SEDs.

3.3. *Galactic Reddening Law for Extragalactic Sources*

The right reddening law for deriving the extinction of any source is one that is monochromatic, because in applying it there is no need to know anything about the spectra of the objects used to derive it. Unfortunately, in one way or another, all reddening laws are founded upon measurements through broadband filters. Thus, they are all object specific. The most problematic are laws constructed by normalizing broadband measurements of extinction to broadband measurements of the optical depth of dust. There is no way to recover monochromatic versions through renormalization if the effective wavelengths to which the extinction coefficients have been assigned

are not consistent with the spectra of the defining sources. In the optical, the coefficients of Cardelli et al. (1989) are derived from extinction measurements in the Johnson system normalized to A_V.

Fitzpatrick (1999) recognized the limitations of existing laws and derived a modern "monochromatic" law from photometry and spectrophotometry of hot stars, taking special care to assign broadband measurements to the effective wavelengths of the filters used to make them. Effective wavelengths were computed by using the SED of an early-type star [$T_{\rm eff} = 30,000$ K, $\log g = 4.0$, $E(B-V) = 0.5$] that was representative of those used to measure the extinction. Even though the law is normalized to $E(B-V)$ (for the SED), it can be converted readily into a completely monochromatic law simply by dividing by the coefficient at some reference wavelength.

The right reddening law for extragalactic sources is the version of a monochromatic law that is applicable to light that traverses a long path through the disk of the Milky Way. In general, the bulk of the extinction will be due to dust in the diffuse component of the interstellar medium. Cores of molecular clouds (in which dust grains may be enlarged) and ionized nebulae (in which small dust grains may have been preferentially destroyed) occupy a small fraction of the volume of the interstellar medium. In addition, they subtend a small angle on the sky. Few galaxies likely to be studied in depth are expected to have their light significantly extinguished by them. Consequently, the appropriate version of the reddening law to use for extragalactic sources is a "normal" one.

Like the reddening law of Cardelli et al. (1989), that of Fitzpatrick (1999) is parameterized in terms of a parameter r to account for the fact that the shape of the law depends upon environment. Fitzpatrick (1999) adopted $r = R_V = 3.1$ to define the "normal" law, characterizing extinction by the diffuse interstellar medium. However, because of effective wavelength shifts, the definition of "normal" is source dependent. In fact, some of the variations in R_V reported in the literature are a consequence of these shifts, not changes in the nature of dust. Traditionally, such variations have been modeled as linear functions of $B-V$ and $E(B-V)$, as in equation (5). Thus, it is logical to compare different measurements of R_V by correcting them to the SED of an A0 V star in the limit of zero reddening, that is, by evaluating R_V^{00}. Such a comparison reveals that the properties of the diffuse interstellar medium over long sightlines are remarkably uniform (McCall & Armour 2000). The most probable value of R_V^{00} is 3.07, with deviations unlikely to exceed 0.05. Consequently, the value of r to use to define a "normal" reddening law appropriate for use with extragalactic sources is that which *delivers* $R_V = 3.07$ when applied to the spectrum of an A0 V star in the limit of zero reddening.

Observed spectra of A0 V stars have limited wavelength coverage, and atmospheric extinction corrections may be imperfect. Instead, following Bessell et al. (1998), the no-overshoot ATLAS9 model spectrum of Vega ($T_{\rm eff}$, $\log g$, $[Z]$, $v_{\rm micro}$) = (9550 K, 3.95, −0.5, 2 km s^{-1}) (F. Castelli 1997, unpublished) was adopted as being representative of an unextinguished star with zero color. The same spectrum was used to determine filter properties given in Table 1. It has the advantage over a directly measured SED in that fluxes are continuously sampled from 0.09 to 160 μm. In addition, the spectrum is unmarred by telluric absorption, which can be accommodated in filter response functions.

The value of r was determined by trial and error. For each choice of r, the reddening law was computed using the algorithm of Fitzpatrick (1999, as communicated by E. L. Fitzpatrick 1999, private communication), and the spectrum was extinguished by $\tau_1 = 0.0001$. Then, using response curves for B and V recommended by Bessell (1990; see § 3.4), A_B and A_V were synthesized from equation (7) to compute R_V. The value of r required to get $R_V = 3.07$ was 3.0408. For all of the work in this paper, the reddening law employed is that of Fitzpatrick (1999) as defined by this choice of r and normalized to the optical depth at 1 μm. It is displayed in Figure 3.

3.4. *Response Functions and Zeropoints*

To facilitate comparisons with previous work on the ratio of total to selective extinction, this paper focuses primarily on filters in the Johnson-Cousins-Glass photometric system (*UBVRIJHK′KLL′M*), for which relative response functions have been defined by Bessell (1990) and Bessell & Brett (1988) and communicated digitally by M. S. Bessell (1999, 2000, private communications).[3] In this paper, the designations *R* and *I* implicitly refer to filters in this system, as against the Johnson system. Each response function is the normalized product of the filter transmission, detector sensitivity and, where warranted, the atmospheric transmission, with edges having been adjusted as necessary until, relative to Vega, synthetic stellar magnitudes derived from spectrophotometry matched measured magnitudes over a wide range of colors. The reflectivity of the telescope optics was approximated as being uniform across each bandpass. Across near-infrared bandpasses, the detector sensitivity was approximated as being unvarying too.

For all filters in the system, photometry of standard stars has been accomplished with current-integrating photomultiplier tubes (see Bessell et al. 1998), and detector sensitivities entering into the response functions were defined on this basis. The implication for this paper is that syntheses must be carried out by integrating energy, that is, by setting $D(\lambda) = 1$.

Software available over the World Wide Web also allows users to compute R_Λ and R'_Λ for Johnson *RI* (i.e., $R_{\rm J} I_{\rm J}$), Sloan Digital Sky Survey (SDSS) *ugriz*, Strömgren *uvby*, Thuan-Gunn *uvgr*, Two Micron All Sky Survey (2MASS) JHK_s, and a wide selection of *Hubble Space Telescope* (*HST*) filters. The response functions for the SDSS, 2MASS, and *HST* filters were adopted from SDSS (2004),[4] Cutri et al. (2003),[5] and Baggett et al. (1997), respectively. Those for the other filters were kindly provided by K. Shimasaku[6] and are described in Fukugita et al. (1995). For the Johnson, Strömgren, and Thuan-Gunn systems, $D(\lambda) = 1$. The SDSS, 2MASS, and *HST*

[3] Note that some of the wavelengths listed for the response function for *M* in Bessell & Brett (1988) are mislabeled. In addition, the tabulated curve is shifted 40 nm with respect to the actual curve.

[4] Funding for the Sloan Digital Sky Survey has been provided by the Alfred P. Sloan Foundation, the Participating Institutions, NASA, the National Science Foundation (NSF), the US Department of Energy, the Japanese Monbukagakusho, and the Max Planck Society. The SDSS Web site is http://www.sdss.org/. The SDSS is managed by the Astrophysical Research Consortium for the Participating Institutions. The Participating Institutions are the University of Chicago, Fermilab, the Institute for Advanced Study, the Japan Participation Group, Johns Hopkins University, Los Alamos National Laboratory, the Max-Planck-Institut für Astronomie, the Max-Planck-Institut für Astrophysik, New Mexico State University, the University of Pittsburgh, Princeton University, the US Naval Observatory, and the University of Washington.

[5] This publication makes use of data products from the Two Micron All Sky Survey (2MASS), which is a joint project of the University of Massachusetts and the Infrared Processing and Analysis Center, funded by NASA and the NSF.

[6] See http://www.astron.s.u-tokyo.ac.jp/~shimasaku.

TABLE 1

PROPERTIES OF FILTERS AS DEFINED BY VEGA

System (1)	Filter (2)	Type (3)	$\lambda_{\rm eff}$ (Å) (4)	$m-V$ (mag) (5)	ζ_ν (mag) (6)	ζ_λ (mag) (7)	R'_Λ (mag) (8)	R_Λ (9)
Bessell	*UX*	C	3663	−0.006	0.775	−0.146	4.453	4.744
Bessell	*BX*	C	4379	−0.002	−0.119	−0.600	3.804	4.053
Bessell	*B*	C	4361	−0.002	−0.118	−0.609	3.820	4.070
Bessell	*V*	C	5448	0.000	0.000	0.000	2.882	3.070
Bessell	*R*	C	6409	0.007	0.179	0.549	2.290	2.440
Bessell	*I*	C	7977	0.003	0.441	1.268	1.609	1.714
Bessell	*J*	C	12211	−0.003	0.901	2.657	0.778	0.829
Bessell	*H*	C	16313	−0.001	1.380	3.760	0.492	0.524
Bessell	*K′*	C	21176	0.000	1.825	4.771	0.337	0.358
Bessell	*K*	C	21871	0.000	1.886	4.906	0.322	0.343
Bessell	*L*	C	34515	−0.008	2.774	6.783	0.174	0.186
Bessell	*L′*	C	38011	−0.008	2.969	7.185	0.154	0.164
Bessell	*M*	C	47911	−0.008	3.430	8.144	0.115	0.122
HST	f300wpc	P	3045	−0.010	1.327	0.014	5.324	5.671
HST	f336wpc	P	3371	−0.010	1.150	0.087	4.768	5.079
HST	f439wpc	P	4310	−0.010	−0.147	−0.668	3.869	4.121
HST	f450wpc	P	4545	−0.010	−0.086	−0.486	3.656	3.895
HST	f555wpc	P	5372	0.000	−0.006	−0.020	2.964	3.157
HST	f606wpc	P	5900	0.000	0.098	0.295	2.602	2.772
HST	f675wpc	P	6687	0.009	0.231	0.673	2.133	2.272
HST	f814wpc	P	7923	0.005	0.416	1.237	1.637	1.744
Johnson	$R_{\rm J}$	C	6688	0.040	0.197	0.669	2.158	2.299
Johnson	$I_{\rm J}$	C	8571	0.060	0.432	1.426	1.443	1.537
SDSS	*u*	P	3607	0.922[a]	−0.038	−0.038[b]	4.506	4.800
SDSS	*g*	P	4672	−0.111[a]	0.002	0.002[b]	3.543	3.775
SDSS	*r*	P	6141	0.138[a]	0.002	0.002[b]	2.422	2.580
SDSS	*i*	P	7458	0.357[a]	0.002	0.002[b]	1.794	1.912
SDSS	*z*	P	8926	0.507[a]	0.022	0.022[b]	1.330	1.417
Strömgren	*u*	C	3462	1.415	−0.315	−1.314	4.650	4.954
Strömgren	*v*	C	4108	0.165	−0.314	−0.941	4.040	4.304
Strömgren	*b*	C	4662	0.004	−0.161	−0.510	3.561	3.793
Strömgren	*y*	C	5454	0.000	−0.004	−0.013	2.857	3.044
Thuan-Gunn	*u*	C	3542	−0.060	1.096	0.140	4.567	4.866
Thuan-Gunn	*v*	C	4014	−0.530	0.558	−0.136	4.123	4.392
Thuan-Gunn	*g*	C	4888	−0.183	0.096	−0.144	3.352	3.571
Thuan-Gunn	*r*	C	6497	0.372	−0.163	0.214	2.225	2.370
2MASS	*J*	P	12285	0.008[c]	0.896	2.662	0.769	0.819
2MASS	*H*	P	16390	0.010[c]	1.376	3.764	0.488	0.519
2MASS	K_s	P	21521	0.013[c]	1.842	4.821	0.329	0.350

NOTES.—Col. (1): Photometric system. Col. (2): Filter designation. Col. (3): Detector characterization (C, current integration; P, photon integration). Col. (4): Effective wavelength, in angstroms. Col. (5): Adopted Pogson magnitude of Vega relative to *V* (for filters redward of *V*, the sign is opposite to that of the color). The apparent Pogson *V* magnitudes adopted for Vega and BD +17°4708 were +0.03 and 9.47, respectively. Col. (6): Magnitude zero point for fluxes in ergs s^{-1} cm^{-2} Hz^{-1}. Col. (7): Magnitude zero point for fluxes in ergs s^{-1} cm^{-2} $Å^{-1}$; Col. (8): A_Λ/τ_1; Col. (9): $A_\Lambda/E(B-V)$.

[a] $m = m_\nu$.

[b] Set equal to ζ_ν.

[c] Derived from fluxes defining $m = 0$.

magnitude systems have been defined by detectors characterized by their response to photons, so $D(\lambda) = \lambda$. Note, however, that the 2MASS response curves have this term built in.

In this paper, source characteristics are quantified through color indices. Color indices are determined for SEDs of interest by measuring effective fluxes. The Pogson magnitude in a particular bandpass is computed from the effective flux per unit wavelength ($F_{\lambda,\rm eff}$) or the effective flux per unit frequency ($F_{\nu,\rm eff}$) using the appropriate zeropoint ζ_λ or ζ_ν. Following Bessell et al. (1998),

$$m_\lambda(\Lambda) = -2.5\log F_{\lambda,\rm eff} - 21.100 - \zeta_\lambda, \quad (14)$$

$$m_\nu(\Lambda) = -2.5\log F_{\nu,\rm eff} - 48.598 - \zeta_\nu, \quad (15)$$

where the units of $F_{\lambda,\rm eff}$ and $F_{\nu,\rm eff}$ are ergs s^{-1} cm^{-2} $Å^{-1}$ and ergs s^{-1} cm^{-2} Hz^{-1}, respectively. Both ζ_λ and ζ_ν are defined to be zero for the *V* band. Values of ζ for other bandpasses are either defined by the colors of Vega ($R_{\rm J}I_{\rm J}$, *HST*, Strömgren, and 2MASS), Vega and Sirius (Johnson-Cousins-Glass), BD +17°4708 (Thuan-Gunn), or are fixed near zero (SDSS). Thus, for all but the SDSS, m_λ is equal to m_ν. The numerical constants in the equations come from requiring that the ATLAS9 model of Vega described above, converted to a flux scale using the angular diameter measured by Hanbury Brown et al. (1974; see Castelli & Kurucz 1994), yields a synthetic magnitude of +0.03 when integrated over the response curve for the *V* band defined by Bessell (1990; see Bessell et al. 1998 for details).

Except for the SDSS and 2MASS systems, zero points were determined by integrating the adopted response functions over SEDs for Vega and BD +17°4708. The SED for BD +17°4708 was taken from Oke & Gunn (1983). Colors for Vega were adopted from Bessell et al. (1998; Johnson-Cousins-Glass), Johnson (1965; Johnson $R_J I_J$), Holtzman et al. (1995) and Fukugita et al. (1995) (*HST*), and Crawford & Barnes (1970; Stromgren). Magnitudes and colors for BD +17°4708 were taken from Kent (1985) and Thuan & Gunn (1976). Note that the colors of Vega adopted for the Johnson-Cousins-Glass system are those forced by the zero points determined by Bessell et al. (1998) through comparison of synthetic colors for both Vega and Sirius with observations (see Table A1 of Bessell et al. 1998). In the case of the SDSS, the relations between magnitude and flux that are currently realized (i.e., for *ugriz*, not $u'g'r'i'z'$) were adopted (SDSS 2004). In the case of 2MASS, the zero points were computed from the zero-magnitude fluxes estimated by Cohen et al. (2003).

Table 1 lists relevant parameters for each filter considered. For the Vega model, it gives the effective wavelengths, the adopted or implied (by ζ) colors relative to *V*, the adopted or implied (by colors) zero points for magnitudes,[7] and values of R'_Λ and R_Λ.

3.5. *Spectral Energy Distributions*

The effective wavelength of a filter is predominantly determined by the shape of the SED across the bandpass. Thus, even for sources that are not heavily obscured optically, the extinction may be very sensitive to the redshift if the ultraviolet flux distribution is not a smooth continuation of the optical. Furthermore, observations of sources that are heavily obscured optically are likely to be focused upon infrared wavelengths. Consequently, for this study, SEDs were required that extended from the space ultraviolet out to beyond the red edge of the *K* band.

3.5.1. *Stars*

SEDs for stars are the foundation of population syntheses, so many libraries exist (see Leitherer et al. 1996). However, most suffer from limited wavelength coverage and/or incomplete sampling of spectral types, luminosity classes, and metallicities. Fortunately, Pickles (1998) created a comprehensive uniform library of stellar SEDs, called HILIB, that suited the needs of this work. The UVKLIB component was employed, which consists of 131 SEDs spanning 1150 to 25000 Å with ~10 Å resolution between 1150 and 10620 Å and 5 Å sampling. At near-solar metallicity, luminosity classes V through I are represented by 36, 14, 32, 8, and 18 SEDs, respectively.

SEDs in HILIB were constructed by averaging data from many sources and are supposed to define the average properties of stars as a function of spectral type and luminosity class. To verify the integrity of the SEDs, and to judge the sensitivity of R_Λ to cosmic scatter, it is valuable to examine spectra of individual stars. Suitable for these tasks is STELIB, a homogeneous library of spectra constructed by Le Borgne et al. (2003) from which HILIB is completely independent. Spectra typically span 3200–9500 Å with 3 Å resolution and 1 Å sampling. Overall, their absolute photometric accuracy is claimed to be 3%. Luminosity classes V through I are covered by 54, 4, 37, 3, and 12 useful spectra (i.e., without gaps), respectively. In this paper, version 3.2 of the library (dated 2003 April 25) is employed. Besides being shifted to the rest frame, all spectra in the library were corrected for extinction by Le Borgne et al. (2003) using the reddening law of Cardelli et al. (1989).

3.5.2. *Galaxies*

The work here was driven primarily by the need for accurate extinction corrections for total magnitudes of galaxies. Thus, truly integrated SEDs spanning a wavelength range like that for the stellar SEDs were required. Furthermore, it was necessary that SEDs for disk galaxies be localized in tilt, so that the impact of inclination on the ratio of total to selective extinction could be evaluated.

Unfortunately, such SEDs did not exist. Integrated spectra acquired by Kennicutt (1992) only go from 3650 to 7100 Å. The SEDs of Coleman et al. (1980), which are commonly used, are constructed from ultraviolet photometry of galaxies subtending angles much larger on the sky than the observing apertures employed. The ultraviolet part of the elliptical template is actually founded upon observations of the cores of the bulges of M31 and M81. Besides the fact that neither is a bare elliptical galaxy, it is recognized that ultraviolet light is more centrally concentrated than visible light in early-type systems (Rifatto et al. 1995b), so core spectra overestimate the ultraviolet contribution to integrated light. Templates for disk galaxies were created by averaging observations of different objects without regard to tilt. It is likely that the SEDs actually do not even represent an ''average'' galaxy, since the effective inclination in the ultraviolet may be lower than in the optical. None of the SEDs extends beyond 1 μm. Similar problems afflict the SEDs of Fukugita et al. (1995). The SEDs defined by Kinney et al. (1996), which have been extended recently out to 2.4 μm (Mannucci et al. 2001), are based upon observations through apertures that are tiny compared with galaxy sizes, so must be regarded as representative only of core properties. Again, one must be concerned about the representation of the ultraviolet relative to the optical. They also are not localized in tilt. Poggianti (1997) used evolutionary synthesis models to produce integrated SEDs for determining *K*-corrections, but their reliability is only as good as the measurements against which they are compared. Furthermore, internal dust is not accommodated.

The needs of this paper forced the creation of new SEDs representative of the integrated light of galaxies with well-defined tilts. For types E, Sab, Sbc, and Im, each SED was constructed from the space ultraviolet to 2.2 μm using integrated photometric and spectroscopic data for a single representative nearby galaxy suffering minimal extinction and with a small to moderate inclination. For type Scd, data for two galaxies with comparable morphology, colors, and tilt were combined. To make it possible to study the ratio of total to selective extinction at *K*, the SEDs were extended to 3.8 μm using measurements of $K-L'$.

Integrated optical spectra have been acquired by Kennicutt (1992), Liu et al. (1999), and Jansen et al. (2000), but few of the galaxies studied by the latter two authors have been comprehensively examined in the space ultraviolet. In the end, SEDs for types E, Sab, Sbc, and Im were built upon observations of NGC 3379, 3368, 5248, and 4449, respectively, integrated spectra for which were acquired by Kennicutt (1992). NGC 3379 is faint in the ultraviolet relative to the optical

[7] Bessell et al. (1998) attempted to summarize the properties of the Johnson-Cousins-Glass system (Table A2 of that paper), but the zeropoints quoted do not reproduce the colors of Vega. Furthermore, zero points by frequency and zero points by wavelength are mistakenly switched.

(Bertola et al. 1982; Rifatto et al. 1995b), so the stellar mix may be relatively homogeneous. Thus, it was felt to be legitimate to incorporate into the elliptical SED small-aperture spectra of this galaxy acquired in the ultraviolet (Oke et al. 1981) and infrared (Mannucci et al. 2001) (the positioning of which was determined by the photometry—see below). Unfortunately, no Scd galaxy could be found for which photometry from the ultraviolet to the infrared in addition to an integrated optical spectrum were available. The SED had to be constructed by combining the integrated optical spectrum of NGC 7620 acquired by Jansen et al. (2000) with integrated photometry for M101 (ultraviolet, B, and I to K_s) and NGC 7620 (U, B, V, and R). Besides being morphologically and photometrically similar, the two contributing galaxies are comparably tilted.

Integrated ultraviolet photometry was extracted from Rifatto et al. (1995a, 1995b), who derived asymptotic magnitudes in three broad spectral regions for a large sample of galaxies by constructing standard luminosity profiles from existing ultraviolet photometry acquired in 20 bandpasses by eight independent experiments (balloons, rockets, and satellites). To improve wavelength resolution, their asymptotic magnitudes were used to estimate total magnitudes for the individual bandpasses from which they were derived. Where a measurement through only one bandpass defined the magnitude for a spectral region, that magnitude was assigned to that bandpass. If the derivation of the asymptotic magnitude employed measurements through more than one bandpass of a given experiment (and aperture), then an asymptotic magnitude was computed for each bandpass by correcting the observation for the difference between the mean magnitude for all of the bandpasses and the adopted asymptotic magnitude for the spectral region.

Beyond I out to 2.2 μm, SEDs were defined by integrated JHK photometry presented in the 2MASS Large Galaxies Atlas, version 2.0 (Jarrett et al. 2003). A measurement of $K-L'$ in the core of NGC 3379 was available to anchor the elliptical SED at longer wavelengths (Impey et al. 1986). For the disk galaxies, $K-L'$ was adopted to be 0.3 ± 0.1, which is what is measured for the cores of elliptical galaxies in the AAO system (Impey et al. 1986; Bessell & Brett 1988). Conversion of $K-L'$ to the 2MASS photometric system was accomplished with the aid of transformation equations in the Explanatory Supplement to the 2MASS All Sky Survey (Cutri et al. 2003).

Photometry for each galaxy was corrected for extinction by employing the estimate for $E(B-V)$ tabulated by NED, which is founded upon K-corrected measurements of colors of elliptical galaxies (Schlegel et al. 1998). Values of τ_1 were determined iteratively from $E(B-V)$ using the elliptical SED. In the optical and infrared, values of R'_Λ were derived iteratively for each galaxy by tuning the corresponding SED to the redshift and optical depth of the galaxy. Because of the narrowness of the bandpasses, extinction corrections for ultraviolet magnitudes were derived simply from the central wavelengths of the filters using τ_1 and the adopted reddening law described earlier.

Ultraviolet magnitudes were corrected for the bandwidth shift accompanying the redshift by subtracting $2.5 \log (1 + z)$. Then they were converted to fluxes per unit wavelength using the zero point specified by Rifatto et al. (1995a). Because most ultraviolet bandpasses were relatively narrow, the wavelengths to which the fluxes were assigned were simply the appropriately blueshifted values of the central wavelengths of the filters employed, as given by Longo et al. (1991) and Rifatto et al. (1995a).

Optical and infrared magnitudes were corrected for redshift by iteratively deriving K-corrections from the SEDs. At L', dm/dz was adopted to be -3 (according to the traditional definition; see Poggianti 1997) based upon analysis of the Vega spectrum in combination with results for the galaxy SEDs at K (see also Impey et al. 1986). Effective fluxes were derived using the zero points given in Table 1. The effective wavelengths to which the fully corrected fluxes were assigned were computed iteratively from each SED using equation (8) with $z = 0$ and $\tau_1 = 0$.

Spectra were corrected for reddening in the same manner as the photometry, with the exception that the monochromaticity of the pixels made it unnecessary to derive extinction coefficients iteratively. Next, they were shifted to the rest frame using velocities measured from the spectra themselves. The atmospheric B band was edited out. Spectra were resampled onto a common grid by fitting splines with a tension of 2.0 (see § 3.6) and averaging the flux under the splines in 5 Å intervals.

The overall shape of each SED was set by fitting splines with a tension of 2.0 to a log-log plot of the fully corrected wavelength-flux pairs defined by the photometry. Owing to the contamination by Hα emission, photometry in R was excluded from the fitting process for the Sbc, Scd, and Im SEDs. Fluxes were normalized to the value interpolated at 5500 Å. Then, each available spectrum was overlaid by shifting in logarithmic flux until the mean was equal to that in the photometric SED over the same range of wavelength. After small adjustments described below, fluxes in the photometric SED were replaced by the fluxes in the spectra where there was overlap. Fluxes beyond the bounds of the spectra were spline interpolated onto the wavelength grid defined by the spectra. The range of wavelength spanned by the SED was determined in the ultraviolet by the bluest photometric or spectral measurement, and in the infrared by the effective wavelength of L'.

In the optical, spectrophotometry is inherently less accurate than photometry. In a relative sense, the calibration at the blue end of a spectrum may be off by up to 10% with respect to the red end (McCall et al. 1985; Jansen et al. 2000), and synthetic colors may deviate accordingly from observed ones. To compensate for calibration uncertainties with a monotonic wavelength dependence, errors in spectroscopic fluxes were approximated to vary as a power law in wavelength, as might be expected if they arose from differential refraction, for example. Except for the elliptical, where color deviations were small, each optical spectrum was merged with the photometry by iteratively twisting it until the synthetic $B-V$ color derived from the merged SED matched that observed. In all cases, an additional small vertical shift was applied to match the synthetic average of $B-I$ and $B-H$ colors ($B-H$ only in the case of the Scd) with the observed average.

The method adopted for aligning spectra and photometry led to significant improvements in the $V-R$ colors of the SEDs; synthetic values are within 0.01 mag of those observed. In addition, it led to $U-B$ colors for the late-type SEDs that are within 0.02 mag of those observed. However, synthetic $U-B$ colors for early-type galaxies remain around 0.15 mag different from the observed values, in part because the rapid change of flux through the U band makes the syntheses critically dependent upon the shape of the response curve adopted, and in part because of the uncertainty in the shape of the SEDs between 3300 and 3600 Å, a region not sampled either photometrically or spectroscopically.

Table 2 summarizes the ingredients of the SEDs and relevant parameters adopted for the galaxies employed in

TABLE 2

OVERVIEW OF THE SEDs

SED (1)	$q^{\rm eff}$ (2)	$V_{\rm rot}^{\rm eff}$ (km s^{-1}) (3)	Source of Spectra (4)	Source of Photometry (5)	Photometry Provided (6)	Type (7)	B_T^0 (mag) (8)	i (deg) (9)	$V_\odot$ (km s^{-1}) (10)	τ_1 (11)	q (12)	$V_{\rm rot} \sin i$ (km s^{-1}) (13)	References (14)
E	0.92	0	N3379	N3379	All	E1	10.11 ± 0.03	...	911	0.0273	0.918	...	
Sab	0.67	252	N3368	N3368	All	SAB(rs)ab	9.96 ± 0.09	50	897	0.0284	0.668	192	I1, Q1, V1
Sbc	0.78	200	N5248	N5248	All	SAB(rs)bc	10.89 ± 0.13	39	1153	0.0273	0.783	146[a]	I1, Q1, V2
Scd	0.95	220	N7620	N5457	uv, *B*, *I*, *J*, *H*, *K*	SAB(rs)cd	8.25 ± 0.09	18	241	0.0102	0.991	68	I2, Q1, V3
				N7620	*U*, *B*, *V*, *R*	Scd	13.42 ± 0.01	19	9582	0.0886	0.946	...	I1, Q1
Im	0.73	85	N4449	N4449	All	IBm	9.98 ± 0.18	50	207	0.0216	0.730	65	I1, Q2, V4

NOTES.—Col. (1): Effective revised Hubble type of SED. Col. (2): Effective apparent axis ratio (b/a) of SED. Col. (3): Effective rotational velocity of SED, derived from $V_{\rm rot} \sin i$. Col. (4): Galaxy defining spectra in SED. Col. (5): Galaxies defining photometry used to construct SED. Col. (6): Photometry defined by galaxy in col. (5). Col. (7): Revised Hubble type, from RC3. Col. (8): Apparent total magnitude in *B*, corrected for Galactic extinction and for redshift via the methods of this paper, but not for tilt. Sources are given in Table 3. Col. (9): Inclination. Col. (10): Heliocentric velocity, from NED. Col. (11): Optical depth at 1 μm, computed using the elliptical SED at $z = 0$ from $E(B-V)$ given by Schlegel et al. (1998) via NED. Col. (12): Apparent axis ratio (b/a). Col. (13): Apparent projected rotational velocity. Col. (14): Sources for i (I), q (Q), and $V_{\rm rot} \sin i$ (V).

[a] Half of W_{20}, the apparent H I line width at 20% of peak.

REFERENCES.—Inclination: (I1) this paper, using q and equation (16); (I2) Bosma et al. 1981. Axis ratio: (Q1) de Vaucouleurs et al. 1991 and Paturel 2004; (Q2) Hunter et al. 1999. Apparent rotational velocity: (V1) Warmels 1988; (V2) Shostak 1978; (V3) McCall 1982; (V4) Hunter et al. 1998, 1999.

constructing them. The inclinations, i, based upon the apparent axis ratios, q, were derived from

$$\cos^2 i = \frac{q^2 - q_0^2}{1 - q_0^2}. \quad (16)$$

Values of q_0, the apparent axis ratio for the edge-on view, were adopted from Bottinelli et al. (1983) and Staveley-Smith et al. (1992). Where possible, the effective rotational velocity associated with a SED was judged from a rotation curve. However, if a galaxy lacked such data, the velocity was derived by correcting its H I line width for turbulence and tilt according to the recommendations of Tully & Fouqué (1985). The effective wavelengths and colors adopted to construct the final SEDs, along with the sources of the photometry, are specified in Table 3.

The SEDs themselves are displayed in Figure 1. Open circles with error bars mark photometric measurements. In the ultraviolet, the SEDs for the elliptical and irregular galaxies are very well defined, so these are used in this paper to explore how the ratio of total to selective extinction depends upon redshift. Sampling in the ultraviolet is not as good for the other SEDs, but it is believed that the level of the ultraviolet relative to the optical is accurately portrayed for each.

3.5.3. *Adjusting for Inclination*

Because the SEDs for disk galaxies were localized in tilt, it was possible to adjust them to approximate SEDs for different tilts. To do so, an analysis like that of Boselli & Gavazzi (1994) was undertaken using a modification of the internal extinction model of Tully & Fouqué (1985). In this model, extinction within a disk galaxy is approximated as being caused by a layer of dust of finite thickness located within the stellar disk. A fraction f of the light of the disk is presumed to be in front of the dust layer, and an identical fraction is presumed to lie behind the layer. If the total optical depth along the line of sight through the dust layer is τ_λ at wavelength λ, then the extinction A_λ^i of the system at inclination i is given by

$$A_\lambda^i = -2.5 \log\left[f(1 + e^{-\tau_\lambda}) + (1 - 2f)\left(\frac{1 - e^{-\tau_\lambda}}{\tau_\lambda}\right)\right]. \quad (17)$$

If the geometry of the layer is approximated to be that of an oblate spheroid with the same shape as the stellar disk, then the apparent optical depth through the layer for the inclined system can be computed from the total optical depth of the dust perpendicular to the midplane, $\tau_\lambda^{i=0}$, and the apparent axis ratio, q (minor relative to major), of the isophotes:

$$\tau_\lambda = \tau_\lambda^{i=0}/q. \quad (18)$$

How $\tau_\lambda^{i=0}$ varies as a function of wavelength is described directly by a reddening law. Using the optical depth at 1 μm as the reference, then

$$\tau_\lambda^{i=0} = \frac{R_\lambda'}{2.5 \log e}\tau_1^{i=0}. \quad (19)$$

Thus, to use equation (17) to convert the SED for a galaxy to a different tilt, it is only necessary to constrain f and $\tau_1^{i=0}$. Except for dwarfs, for which the effects of tilt on the light are minimal anyway, it is reasonable to presume that the law governing internal reddening globally is similar to the one describing reddening by the diffuse interstellar medium in the Milky Way.

In a given bandpass, the total extinction due to internal dust is not well constrained. However, broadband colors can be used to derive how the extinction changes differentially as a galaxy is tilted, which is what is relevant to this work. It is usual to describe the internal extinction of an inclined galaxy as an excess over what is observed face-on:

$$A_\lambda^{i-0} = A_\lambda^i - A_\lambda^{i=0}. \quad (20)$$

For a broadband filter Λ, the extra extinction A_Λ^{i-0} of a galaxy at inclination i can be determined for an arbitrary tilt by first correcting the representative SED to face-on using equations (17)–(20) and then computing the effective flux (eq. [6]). The excess extinction for inclination i then follows by using the same equations to correct the face-on SED to the desired tilt and then comparing the effective flux for that tilt to the face-on value. For bandpasses Λ_1 and Λ_2, the excess reddening follows from

$$E(\Lambda_1 - \Lambda_2)^{i-0} = A_{\Lambda 1}^{i-0} - A_{\Lambda 2}^{i-0}. \quad (21)$$

In order to derive how tilt affects broadband magnitudes of spirals, Tully et al. (1998) examined galaxies in the Ursa Major and Pisces Clusters to measure how $B-K'$, $R-K'$, and $I-K'$ change as a function of q. They derived the relationship between A_Λ^{i-0} and $\log q$ for each of B, R, I, and K' by assuming $A_\Lambda^{i-0}/A_B^{i-0}$ is a constant. Corrections were shown to depend upon luminosity, as characterized by the H I line width.

The correction formulae of Tully et al. (1998) were used here to derive f and $\tau_1^{i=0}$ and thereby obtain, through equations (17) and (20), a general prescription for adjusting the SED of a galaxy for tilt. The Sbc SED was adopted as being representative of the galaxies studied by Tully et al. (1998). Solutions for f and $\tau_1^{i=0}$ were derived by nonlinear least squares. Iteratively, for each choice of f and $\tau_1^{i=0}$, one or more of $B-K'$, $R-K'$, and $I-K'$ were synthesized for the face-on view and then compared with syntheses for tilts deviating from face-on. The deviations of the colors from the face-on values were compared with those predicted by the formulae of Tully et al. (1998), and iterations were continued until the variance of the residuals was minimized. Luminosity dependences were accommodated via rotational velocities, which have the advantage of being independent of distance.

Fits to individual colors revealed that f had to increase with wavelength, just as found by Boselli & Gavazzi (1994). This is not surprising if one considers that younger stars, for which the scale height is lower, contribute proportionally more to the light at shorter wavelengths. In addition, both f and $\tau_1^{i=0}$ had to vary with the rotational velocity to account for the dependence of A_Λ^{i-0} on H I line width. In the end, the following relations were derived from a simultaneous fit to all three colors for q ranging from 0.25 to 0.75 (i from 81° to 42°) and for rotational velocities ranging from 100 to 250 km s^{-1}:

$$f = 0.165 + 0.370 \log(\lambda/1\ \mu\text{m}) - 0.412 \log\left(V_{\rm rot}/200\ \text{km s}^{-1}\right), \quad (22)$$

$$\tau_1^{i=0} = 0.624 + 1.316 \log\left(V_{\rm rot}/200\ \text{km s}^{-1}\right). \quad (23)$$

Here λ is the wavelength in microns and $V_{\rm rot}$ is the rotational velocity (i.e., in the plane of the disk) in kilometers per second. Negative occurrences of f or $\tau_1^{i=0}$ are replaced by zero.

TABLE 3

ADOPTED PHOTOMETRY FOR SEDs

	E			Sab			Sbc			Scd			Im		
FILTER[a] (1)	$\lambda_{\rm eff}$ (2)	$(m-B)^0_T$ (3)	Ref. (4)	$\lambda_{\rm eff}$ (5)	$(m-B)^0_T$ (6)	Ref. (7)	$\lambda_{\rm eff}$ (8)	$(m-B)^0_T$ (9)	Ref. (10)	$\lambda_{\rm eff}$ (11)	$(m-B)^0_T$ (12)	Ref. (13)	$\lambda_{\rm eff}$ (14)	$(m-B)^0_T$ (15)	Ref. (16)
1330.....	1326	2.911 ± 0.15	1, 3	...	...	...	...	...	...	...	...	...	...	...	...
1550.....	1545	3.793 ± 0.15	1, 3	1545	1.480 ± 0.26	2, 3	1544	-0.223 ± 0.18	2, 3	1549	-1.833 ± 0.36	2, 3	1549	-1.461 ± 0.34	2, 11
1800.....	1795	3.789 ± 0.15	1, 3	1795	1.566 ± 0.26	2, 3	1793	-0.388 ± 0.18	2, 3	...	...	...	...	...	...
1910.....	...	...	...	...	...	...	...	...	...	1908	-1.324 ± 0.36	2, 3	1909	-0.993 ± 0.22	2, 11
2200.....	2193	3.647 ± 0.14	2, 3	...	...	...	2192	0.142 ± 0.57	2, 3	...	...	...	...	...	...
2460.....	...	...	...	2453	2.248 ± 0.13	2, 3	...	...	...	2458	-0.572 ± 0.77	2, 3	2458	-0.667 ± 0.21	2, 11
2980.....	...	...	...	2971	0.893 ± 0.12	2, 3	...	...	...	...	...	...	2978	-0.553 ± 0.12	2, 11
3300.....	3290	1.330 ± 0.15	2, 3	...	...	...	3287	-0.315 ± 0.36	2, 3	...	...	...	...	...	...
3320.....	...	...	...	3310	0.817 ± 0.20	2, 3	...	...	...	...	...	...	3318	-0.472 ± 0.07	2, 11
UX.....	3685	0.500 ± 0.01	4, 5	3668	0.282 ± 0.02	4, 9	3612	0.030 ± 0.01	4, 5	3630	-0.163 ± 0.05	10	3625	-0.367 ± 0.01	4, 12
B.....	4496	0.000 ± 0.03	4, 5	4472	0.000 ± 0.09	9	4434	0.000 ± 0.13	4, 5	4408	0.000 ± 0.09	4, 5, 10	4396	0.000 ± 0.18	12
V.....	5532	-0.928 ± 0.01	4, 5	5519	-0.797 ± 0.05	9	5512	-0.620 ± 0.01	4, 5	5490	-0.417 ± 0.04	4, 5	5487	-0.389 ± 0.01	12
R.....	6570	-1.508 ± 0.01	6	6554	-1.298 ± 0.03	9	6545	-1.101 ± 0.02	6	6518	-0.774 ± 0.05	10	6516	-0.786 ± 0.01	13
I.....	8038	-2.119 ± 0.01	6	8038	-1.889 ± 0.03	9	8045	-1.654 ± 0.03	6	8019	-1.306 ± 0.19[c]	4, 5	8026	-1.162 ± 0.19	12
J.....	12374	-2.956 ± 0.02	7	12368	-2.748 ± 0.02	7	12381	-2.731 ± 0.02	7	12361	-1.741 ± 0.03	7	12364	-1.892 ± 0.03	7
H.....	16424	-3.625 ± 0.02	7	16436	-3.406 ± 0.02	7	16434	-3.436 ± 0.02	7	16446	-2.450 ± 0.04	7	16432	-2.533 ± 0.03	7
K_s.....	21532	-3.835 ± 0.02	7	21542	-3.645 ± 0.02	7	21538	-3.635 ± 0.03	7	21545	-2.740 ± 0.05	7	21539	-2.732 ± 0.04	7
L'[b].....	38011	-4.056 ± 0.07	8	38011	-3.905 ± 0.10	...	38011	-3.895 ± 0.11	...	38011	-3.000 ± 0.11	...	38011	-2.992 ± 0.11	...

NOTES.—Col. (1): Filter. Cols. (2), (5), (8), (11), and (14): Effective wavelength for bandpass, in angstroms. Cols. (3), (6), (9), (12), and (15): Total magnitude m for the specified bandpass with respect to B, corrected for Galactic reddening and for redshift via the methods of this paper, but not for tilt. Note that the sign is opposite to that of the color for bandpasses redward of B. Uncertainties are for m alone, i.e., they do not include the uncertainty in B. Cols. (4), (7), (10), (13), and (16): Sources of magnitudes (or colors) and errors.

[a] Tabulated magnitudes lie in the following systems: 1330 through 3320, IUE (Rifatto et al. 1995a); *UX*, *B*, *V*, *R*, *I*, L', Bessell (Bessell & Brett 1988; Bessell 1990; Bessell et al. 1998); and *J*, *H*, K_s, 2MASS (Cohen et al. 2003).

[b] On the system of Bessell, $(K-L')^0$ was adopted to be 0.30 ± 0.10 for all but E (Impey et al. 1986), which becomes 0.26 once K is converted to the 2MASS system (Cohen et al. 2003). The value of $\lambda_{\rm eff}$ for L' is that for the model spectrum of Vega (see text).

[c] From $(V-I)_e$ and $(B-V)_T$ for N5457.

REFERENCES.—(1) Longo et al. 1991; (2) Rifatto et al. 1995a; (3) Rifatto et al. 1995b; (4) de Vaucouleurs et al. 1991; (5) Paturel 2004; (6) Buta & Williams 1995; (7) Jarrett et al. 2003; (8) Impey et al. 1986; (9) Macri et al. 2000; (10) Jansen et al. 2000; (11) Code & Welch 1982; (12) Makarova 1999; (13) Swaters & Balcells 2002.

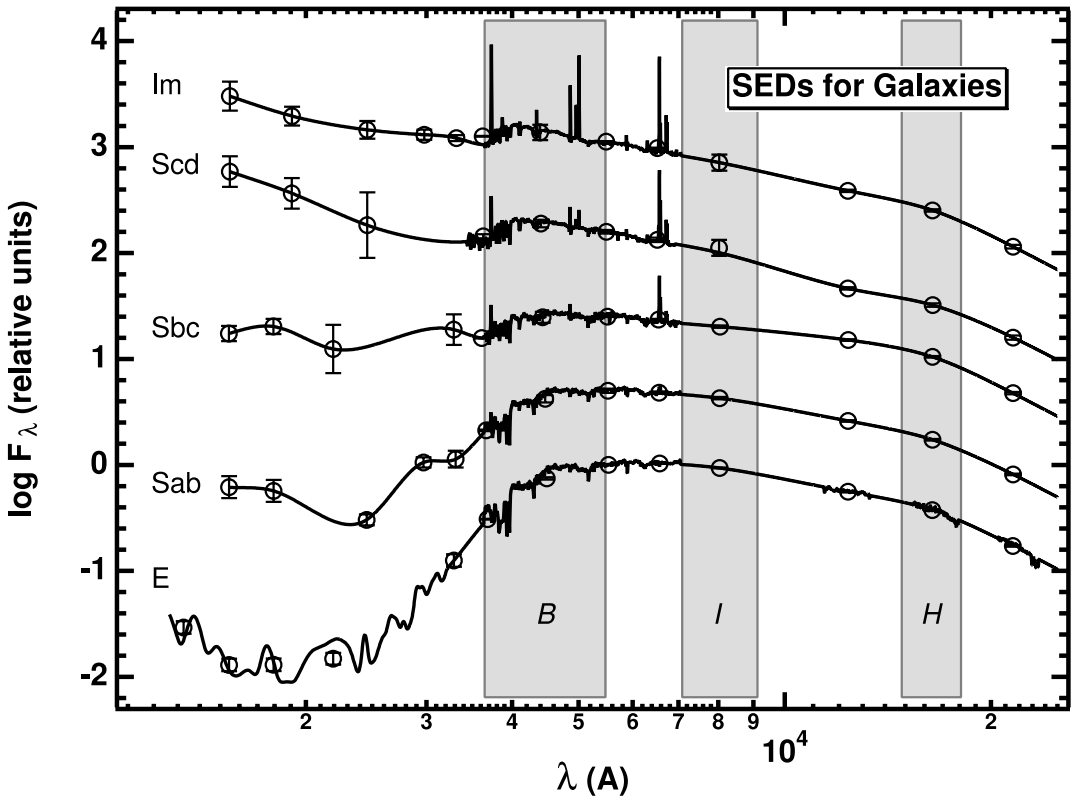

FIG. 1.—Integrated SEDs for galaxies. Each shaded region delineates where the response in a bandpass (B, I, or H) exceeds 1% of the peak for that bandpass. Open circles mark fluxes derived from photometry. Except for B, error bars give uncertainties with respect to B, i.e., excluding the uncertainty in B.

Figure 2 compares the resulting values of $E(\Lambda - K')^{i-0}$ and A_Λ^{i-0} with those of Tully et al. (1998) for $V_{\rm rot} = 250$ km s^{-1} [for which $E(\Lambda - K')^{i-0}$ and A_Λ^{i-0} are largest]. In the left panel, the vertical dashed lines bound the range of q over which the fits to $E(\Lambda - K')^{i-0}$ were made. Over the entire range of rotational velocities fitted, synthesized color corrections are nearly all within 0.03 mag of those recommended by Tully et al. (1998). Nevertheless, the right panel shows that for $q < 0.6$ the new values of A_Λ^{i-0} are systematically higher than recommended by Tully et al. (1998), by up to 0.13 mag at $q = 0.25$. This is because $A_\Lambda^{i-0}/A_B^{i-0}$ is not a constant for any filter, and at large inclinations it rises higher than the values guessed by Tully et al. (1998). For example, Tully et al. (1998) adopted $A_{K'}^{i-0}/A_B^{i-0} = 0.14$ (as implied by their relations). Here, for $V_{\rm rot} = 250$ km s^{-1}, the ratio ranges from a value of 0.14 near face-on to 0.22 at $q = 0.25$.

Figure 3 compares the adopted reddening law for the diffuse interstellar medium with that implied by equations (17), (22), and (23) for a galaxy with $V_{\rm rot} = 200$ km s^{-1} and $q = 0.25$. For the tilted galaxy, the reddening coefficients were computed from

$$A_\lambda/\tau_1 = (2.5 \log e)(A_\lambda^{i-0}/A_1^{i-0}). \quad (24)$$

Tilt leads to comparatively little excess extinction in the optical and ultraviolet relative to that in the near-infrared. The curve for the tilted galaxy is actually reminiscent of that for star-forming regions where $R_V \gg 3$, even though the reddening law for the diffuse interstellar medium is behind it. It is the declining value of f toward the ultraviolet that causes the difference. The kink at $\sim$3600 Å marks where f drops to zero (and is forced to remain zero blueward of that point).

The value of $\tau_1^{i=0}$ reaches zero at $V_{\rm rot} = 67$ km s^{-1}, which is reasonable considering that metallicities in dwarfs are low. The surprising result is the high value of $\tau_1^{i=0}$ at rotational velocities typical of giant spirals. For an Sbc galaxy with $V_{\rm rot} = 200$ km s^{-1}, it implies a face-on extinction of 0.95 mag in B, which is unlikely, although consistent with the findings of Boselli & Gavazzi (1994). This suggests that the extinction model described by equations (17), (22), and (23) is imperfect, and that derived values of A_λ^{i-0} should be treated with considerable caution. Nevertheless, it reasonably describes the behavior of colors with tilt over a wide range of wavelength and should be legitimately usable to adjust the SED of a disk galaxy for tilt between 0.4 and 2.2 μm.

3.6. *Numerical Approach*

All interpolations and integrations required to compute A_Λ for a given set of inputs were accomplished by connecting points with splines under tension. The required subroutines were taken from the FITPACK library (Cline 1989). Tense splines differ from cubic splines in that the weighting of the first derivatives, which determine the curviness of the resulting function, is adjustable. This helps to avoid the extreme fluctuations that can arise when true cubic splines are fit to noisy data. As the tension parameter approaches zero (e.g., 0.001), the function approaches the shape expected for a cubic spline. As the tension parameter becomes large (e.g., 50), the function comes close to that of a polygonal line. Typically, the tension parameter is selected to be unity.

To compute the integrands in equation (6), a uniform 2 Å grid of wavelengths was created that spanned the range of definition of the response function. The mean response in each bin was determined by integrating under an interpolating

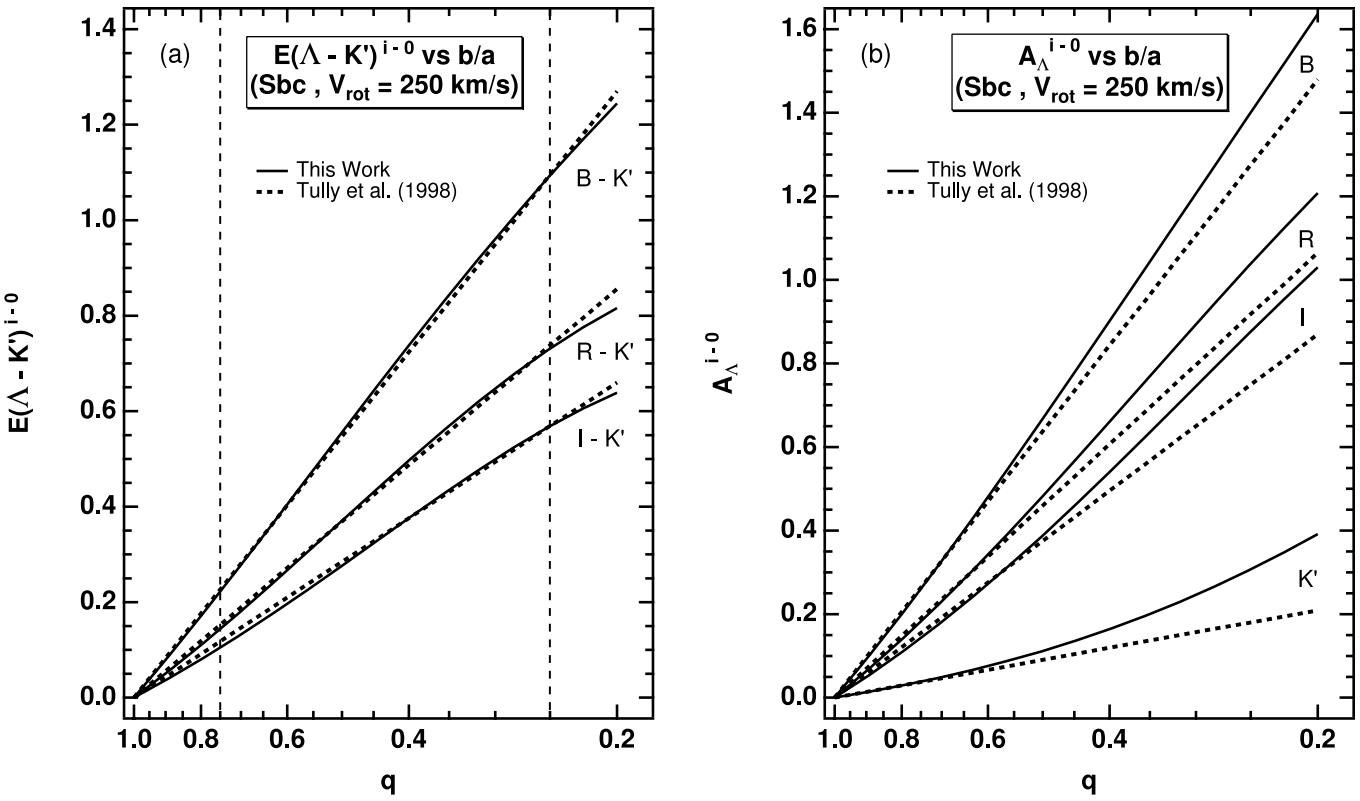

FIG. 2.—Dependence upon the apparent axis ratio q of (*a*) the excess reddening over face-on and (*b*) the excess extinction over face-on for an Sbc galaxy at $z = 0$ rotating at 250 km s^{-1}. The solid curves were derived in this work, and the dotted curves show the corresponding predictions of Tully et al. (1998). In the left panel, the vertical dashed lines bound the range of q over which the fits of $E(\Lambda-K')^{i-0}$ to the predictions of Tully et al. (1998) were made. For $q < 0.6$, the fits demand somewhat higher values of A_Λ^{i-0} than predicted by Tully et al. (1998).

spline. To safely handle poor sampling, the tension of the spline was set to 10.0. The chosen SED was resampled to the same grid by integrating 2 Å intervals under an interpolating spline defined by a tension of 2.0. To duplicate Fitzpatrick (1999), the coefficients of the reddening law were interpolated to the grid wavelengths using a spline with a tension of 1.0. The first derivatives at the endpoints of the response curve and of the SED were set to zero, but those for the reddening law were estimated from the coordinates of the first and last three points.

4. RESULTS

4.1. $A_V/E(B-V)$ *versus Color and Optical Depth*

Figure 4 shows how R_V varies with $(B-V)^0$ (*left*) and $(B-I)^0$ (*right*) for stars at rest in the limit of zero reddening. The plotted colors are the synthetic values at zero optical depth and zero redshift. For each luminosity class, a curve connects HILIB SEDs in order of spectral type. In the case of late-type giants, $(B-V)^0$ is not a good sequencing index, and the curve turns back on itself; $(B-I)^0$ is superior. In each panel, the horizontal dashed line marks the adopted value of R_V^{00} (see § 3.3). Clearly, R_V for most stars is substantially greater. Along the main sequence, it increases from 3.0 at $(B-V)^0 = -0.4$ (O5 V) to 3.7 at $(B-V)^0 = 1.8$ (M6 V), a change of 23%.

In the right panel, individual stars in the STELIB library are marked with symbols distinguished on the basis of the luminosity classes advertised by Le Borgne et al. (2003). There is excellent agreement between the HILIB tracks and the STELIB points, verifying the integrity of the HILIB templates. Furthermore, the range of variation of R_V in each luminosity class far exceeds the scatter at any given color. Relative to the solar system, metallicities for stars in the STELIB database vary by 2 orders of magnitude. Whatever effect the variations have on R_V must be insignificant compared with that due to changing spectral type.

Beyond $(B-I)^0 \sim 2.0$ (K2 V), R_V at a given color becomes quite sensitive to the luminosity class. Out to $(B-I)^0 \sim 4$ (M3 V), R_V for evolved stars rises up to 7% higher than what is seen for dwarfs. However, at redder colors, R_V for giants drops as low as 17% below expectations for dwarfs. Figure 7*b* reveals that dwarfs and giants have similar values of R_V', so the differences in R_V must originate in the B band.

The inclined dashed line in Figure 4*a* shows the expected variation of R_V according to Schmidt-Kaler (1982; eq. [5]). It tracks reality reasonably only out to $(B-V)^0 \sim 0.2$ (A7 V). Olson (1975) points out that equation (5) also should break down at extinctions exceeding about 5 mag in V.

Galaxies are composed of many different kinds of stars. Figure 5 compares the integrated SED of an Sbc galaxy at rest (derived in § 3.5) with that of a G2 V star (Pickles 1998) which has the same synthetic $B-V$ color (0.65 vs. 0.62 for the Sbc galaxy). For reference, the extents of the B, V, and I bandpasses within which the response exceeds 1% of the peak are shown (Bessell 1990). Even though the colors are the same, syntheses reveal that R_V is 3.08 for the Sbc galaxy, but 3.18 for the G2 V star (in the limit of zero reddening). Hot stars in the galaxy have altered the distribution of flux across the B band, shifting the effective wavelength blueward of that for the star. As a result, for a given column of dust, A_B is higher relative to A_V, and R_V is reduced.

Figure 6 shows how R_V varies with $(B-V)^0$ (the synthetic $B-V$ color at zero optical depth and zero redshift) for galaxies

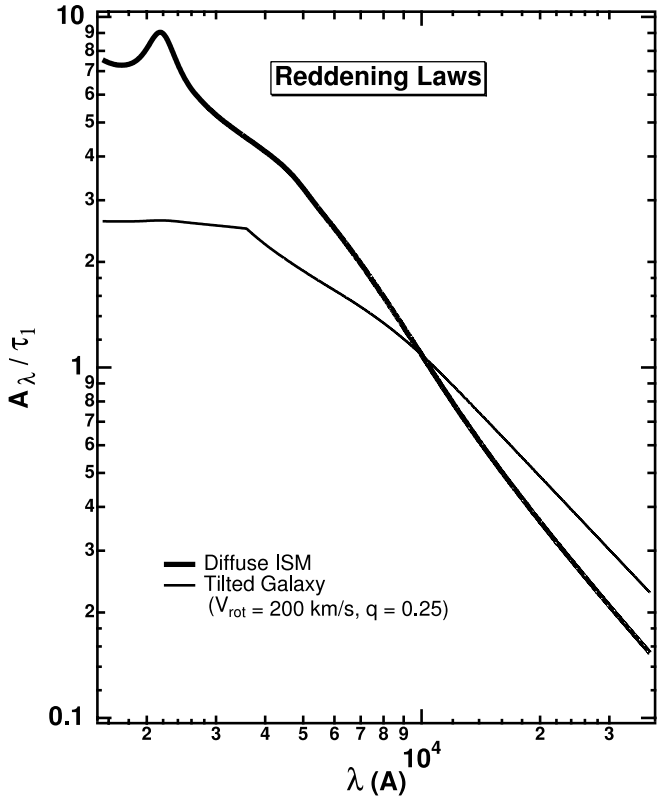

FIG. 3.—Reddening laws. The coefficients on the ordinate give the extinction at wavelength λ normalized to the optical depth at 1 μm. The thick curve gives the adopted law for the diffuse interstellar medium of the Milky Way. It delivers $R_V = 3.07$ when integrated over the spectrum of Vega. The thin curve is the effective law of reddening relative to face-on for a highly tilted galaxy ($q = 0.25$), based upon a model that matches how broadband colors vary with the apparent axis ratio. The bump at 3600 Å is an artifact of the model (see text).

at rest. The solid curve shows the variation in R_V along the Hubble sequence, as indicated by the SEDs created for this paper (without any adjustment for tilt). The dotted curve shows how R_V varies along the HILIB main sequence out to spectral type M2.5 V. Open circles mark normal galaxies observed by Kennicutt (1992; corrected for reddening and redshift, but not for tilt), and open triangles denote main-sequence stars in the STELIB library. Because of the limited wavelength coverage of the spectra of Kennicutt (1992; 3650 to 7100 Å), all syntheses for Figure 6 were performed using slightly modified B and V response curves; the blue edge of the standard response curve for B was moved from 3600 to 3660 Å, and the red edge of the response curve for V was moved in from 7400 to 7030 Å. Nevertheless, resulting colors are very close to those derived using the standard curves.

Despite the limitations of $(B-V)^0$ as a sequencing index for galaxies (see below), there is clearly a systematic variation in R_V along the Hubble sequence that is different from that seen along the main sequence. The range of variation far exceeds the scatter in measurements for individual galaxies at a given color, which comes from a combination of uncertainties in spectral flux calibrations, variations in the amount of obscuration by internal dust, and cosmic scatter in spectral properties. Certainly, the trend along the Hubble sequence is described reasonably by the SEDs derived here.

Note that no Scd galaxies were observed by Kennicutt (1992), so it is not possible to decide whether the small discrepancy between the result for the Scd template and those for individual galaxies of comparable color, but earlier type, is a peculiarity of the template.

For composite populations, $(B-I)^0$ is superior to $(B-V)^0$ in sequencing the ratio of young to old stars. In addition, it is not affected by Hα emission, which falls at the red edge of the V band. In addition, as evidenced by Figure 4, $(B-I)^0$ varies more smoothly with spectral type than $(B-V)^0$ for late-type giant stars, which dominate the light of old populations. Figure 7 shows for galaxies at rest how R_V (*left*) and R'_V (*right*) vary with $(B-I)^0$ (the synthetic $B-I$ color at zero optical depth and zero redshift) and with the optical depth of Galactic dust. As before, the adopted SEDs are as originally constructed, that is, not adjusted to face-on. Loci for HILIB main-sequence and giant stars are superposed.

In each panel, points for galaxies are connected with a thick solid line in order of Hubble type. Points for main-sequence stars are connected with a thick dotted line in order of spectral type. A thin solid line connects points for giants in order of spectral type. For galaxies and main-sequence stars, results are presented for two choices of τ_1, namely, in the limit as τ_1 approaches zero and for $\tau_1 = 2$. The thin dotted curve coming out of the Hubble sequence shows how the point for the Sbc SED moves as the tilt is increased (to $q = 0.2$; see § 4.2).

Along the Hubble sequence, R_V changes by 5%, much less than is the case for the full range of stellar spectral types. For the elliptical SED in the limit of zero reddening, $R_V = 3.20$. In comparison, using a reddening law for the diffuse interstellar medium constructed from functions provided by O'Donnell (1994) and Cardelli et al. (1989), Schlegel et al. (1998) computed $R_V = 3.315$ (for a somewhat different rendition of the Johnson-Cousins system). Except at the elliptical end, values of R_V lie systematically below those for main-sequence stars. The deviation is greatest (5%) for intermediate- to late-type galaxies. Yet, Figure 7*b* reveals that A_V/τ_1 is the same for galaxies as for stars. This shows that the divergence in R_V is a consequence of the inhomogeneous mix of stars contributing to the flux in the B band [which affects $E(B-V)$]. Note that a 5% error in R_V leads to a *systematic error* of 0.25 mag for $A_V = 5$.

Surprisingly, R_V for elliptical galaxies lies about 4% below the value for giants of the same color, even though giants probably dominate the light. The discrepancy must be due to the contribution of a wide range of spectral types to the light in the B band. Clearly, it is inadvisable to use R_V for color-matched giants to correct the integrated light of an elliptical galaxy for extinction.

Figure 7*b* shows that the trend of R'_V with color is opposite to that of R_V. Thus, how R_V varies is being determined primarily by what happens to $E(B-V)$ as effective wavelengths shift. The variation of $E(B-V)/\tau_1$ with color can be seen in Figure 8*a*.

For both stars and galaxies, the sensitivity of R_V and R'_V to Galactic extinction is weak. Even with $\tau_1 = 2$ ($A_V \sim 5.5$), R_V is increased by 1% at most, and R'_V is decreased by 2%. In fact, for stars the sensitivity of R_V to τ_1 is much weaker than suggested by Schmidt-Kaler (1982; see the next section).

4.2. $A_V/E(B-V)$ *for Galaxies versus Tilt*

To examine how R_V for galaxies varies with tilt, the rest-frame Sbc SED was modified according to the algorithm developed in § 3.5.3 to reflect that of a galaxy viewed at various angles conveyed by axis ratios q ranging from face-on (1.0) to near edge-on (0.2). Figure 9*a* shows how R_V varies with q, and Figure 9*b* displays how R_V is correlated with the *apparent*

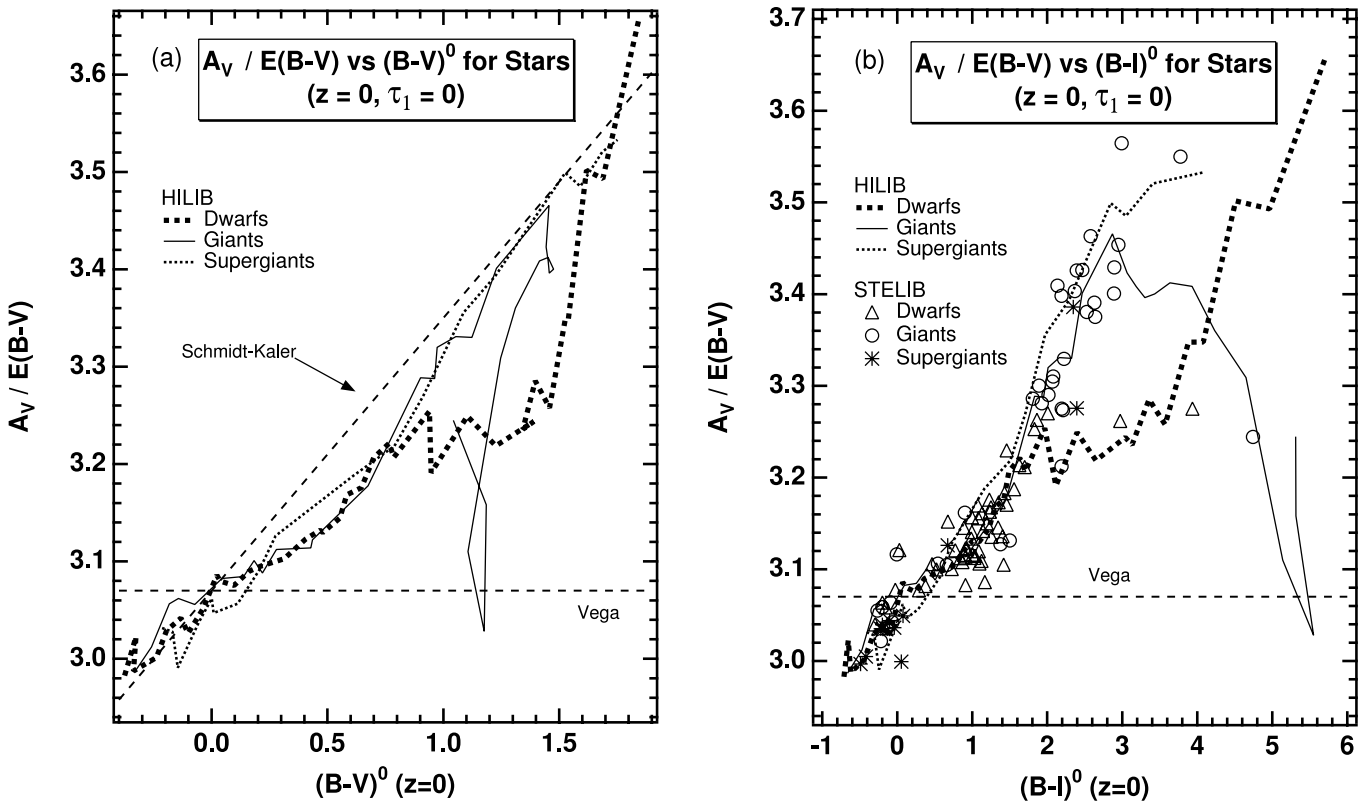

FIG. 4.—R_V vs. (*a*) $(B-V)^0$ and (*b*) $(B-I)^0$ for stars at zero redshift ($z = 0$) in the limit of zero reddening ($\tau_1 = 0$). For each luminosity class, a curve sequences SEDs in the HILIB library by spectral type. The inclined dashed line in the left panel displays the trend predicted by Schmidt-Kaler (1982). In the right panel, individual stars in the STELIB library are plotted, also using different symbols for different luminosity classes. In each panel, the horizontal dashed line is the adopted value of R_V for Vega (R_V^{00}).

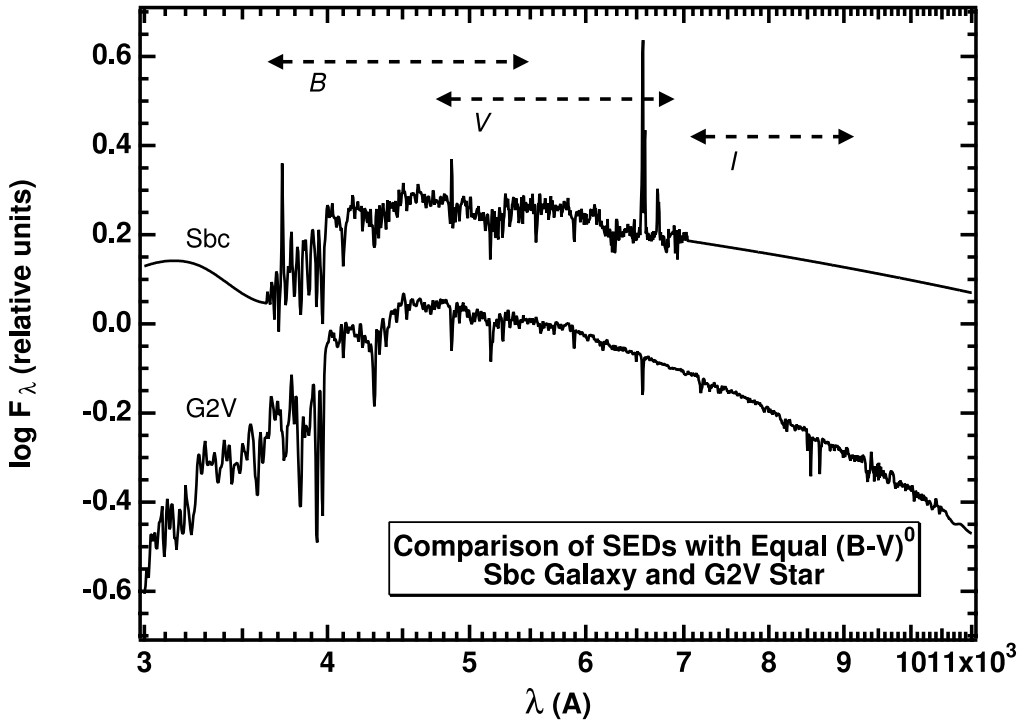

FIG. 5.—SEDs for an Sbc galaxy and a G2 V star with the same $B-V$ color. For each of *B*, *V*, and *I*, a horizontal dashed line marks the range in wavelength over which the filter response exceeds 1% of the peak response.

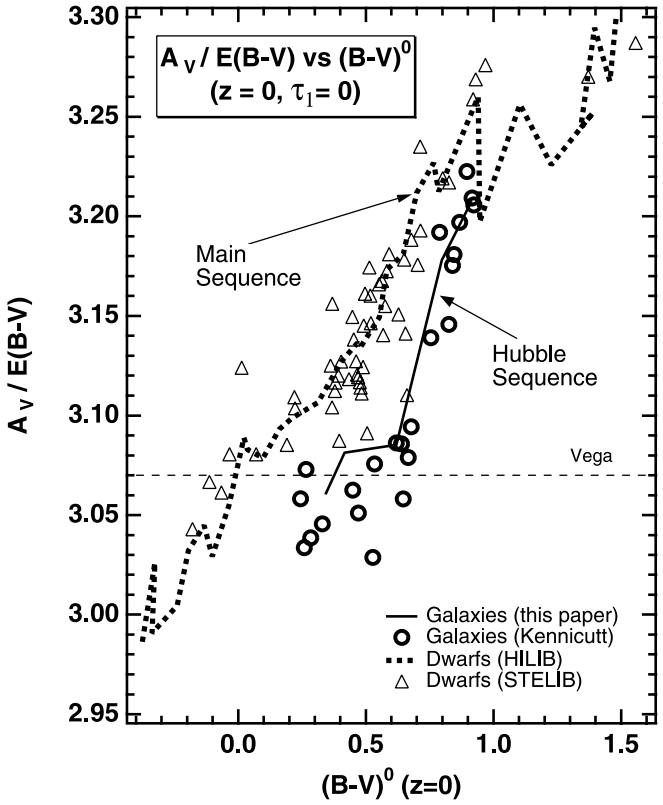

FIG. 6.—R_V vs. $(B-V)^0$ for stars and galaxies at zero redshift ($z = 0$) in the limit of zero reddening ($\tau_1 = 0$). The dotted curve connects results for HILIB main-sequence SEDs in order of spectral type. Open triangles mark main-sequence stars in the STELIB library. The solid curve sequences results for the galaxy SEDs generated for this paper in order of Hubble stage. Open circles show results for individual normal galaxies observed by Kennicutt (1992). SEDs for the galaxies were not adjusted in any way for tilt. The horizontal dashed line is the adopted value of R_V for Vega in the rest frame.

$B-V$ color. How R_V correlates with the apparent $B-I$ color is shown in Figure 7*a* as a thin dotted curve emanating from the Hubble sequence. The track for R'_V in Figure 7*b* falls right on top of the Hubble sequence, so it cannot be seen. Also shown in Figure 9*b* is the relationship between R_V and $B-V$ which comes about for a face-on Sbc galaxy as the optical depth of foreground dust is increased.

The figures show that R_V is not very sensitive to tilt. Even for an edge-on system ($q = 0.2$), it is predicted that R_V should be only 1% larger and R'_V only 0.4% smaller than estimated for the face-on view, which is significantly less than the range of variation along the Hubble sequence. Interestingly, Figure 9*b* shows that the correlation of R_V with $B-V$ caused by tilt is much steeper than that arising from the imposition of dust in the foreground. The correlation for foreground dust advocated by Schmidt-Kaler (1982) for stars (eq. [5]) is shown as a dashed line. It lies about halfway between the two curves.

4.3. $A_V/E(B-V)$ *versus Redshift and Optical Depth*

Sensitivities of R_V and R'_V to redshift and optical depth have been derived for two important classes of stars. Results are displayed in Figure 10. The two panels focus on luminous stars that are or are likely to become targets of study out to great distances: a Type Ia supernova 3 days after maximum light (with a stretch of 1.0) and a G8 supergiant, the latter meant to be representative of a long-period Cepheid variable. The left panel (R_V) would be employed to judge extinction if the color excess due to Galactic dust could be judged from the intrinsic color and K-corrections. The right panel (R'_V) would be used if the optical depth of dust in the Milky Way could be judged by independent means, say from the maps of Schlegel et al. (1998). Note that the redshift range of the left panel is half that of the right because the spectral coverage limits syntheses in B. The SED employed for the supergiant is from HILIB and that for the supernova is from Nugent et al. (2002). Nugent et al. (2002) have already realized the significance of the ratio of total to selective extinction to supernovae cosmology and have shown, in particular, that the ratio of total to selective extinction is very sensitive to phase. However, they have not explicitly shown how the ratio varies with redshift.

For both kinds of stars, R_V varies strongly with redshift, by 16% in the case of the supernova and 22% in the case of the supergiant out to a redshift of 0.4. Out to a redshift of 0.3, the trend for the supernova is for extinction corrections at a given $E(B-V)$ (due to Galactic dust) to increase. On the other hand, there is an overall decline in R'_V with redshift. In addition, the sensitivity to redshift is weaker than for R_V, with the range of variation amounting to 3% for the supernova and 5% for the supergiant out to a redshift of 0.4.

The thinnest solid and dotted curves in Figure 10 show what happens to R_V and R'_V if there is intervening dust either in the Milky Way (Galactic dust) or in the frame of reference of the stars (localized dust) with an optical depth at 1 μm of 2.0. Shifts vary with redshift, although overall trends with redshift remain intact. Notably, R'_V is more sensitive to localized dust than it is to Galactic dust. The reason why the curves for localized dust do not overlap with those for Galactic dust at $z = 0$ is because R_V and R'_V [i.e., A_V, $E(B-V)$, and τ_1] apply specifically to dust in the Milky Way. A SED reddened by localized dust with some optical depth is affected differently by Galactic dust than is a SED that starts off unreddened but that is obscured by the same optical depth of Galactic dust. For example, R'_V is lower because the effective wavelength of V is redder.

Derived values of $E(B-V)$ for a given supernova SED will change with redshift (owing to the changing K-corrections), so it is difficult to interpret the consequences of Figure 10*a* for cosmology. What is important is to judge the implications of adopting a fixed estimate of the color excess due to Galactic dust, as might be gleaned from a map like that of Schlegel et al. (1998), along with a fixed ratio of total to selective extinction. This can be accomplished with the aid of Figure 10*b*. Fixing the color excess is akin to fixing the optical depth of intervening dust, since it is a quantity that is independent of the redshift of the supernova. Thus, how R'_V varies with redshift determines the size of errors associated with adopting a fixed value of R_V.

Figure 10*b* shows that R'_V for the supernova *declines* by 0.11 (4%) out to a redshift of 0.5, which is where residuals supporting accelerating universal expansion reach a maximum of about 0.25 mag with respect to expectations for unaccelerated expansion (Riess et al. 2004). If R'_V were fixed and applied to evaluate A_V from a fixed value of $E(B-V)$, supernovae at $z \sim 0.5$ would end up brighter than they ought to be relative to nearby ones, opposite to what is observed. Of course, the true picture would depend upon the actual values of $E(B-V)$ adopted for different fields. In V, to reduce errors due to the variation in R'_V to less than 10% of the observed residuals (0.025 mag), it is necessary to restrict attention to fields for which τ_1 is less than about 0.2. Note that supernovae SEDs do not extend far enough into the ultraviolet to judge

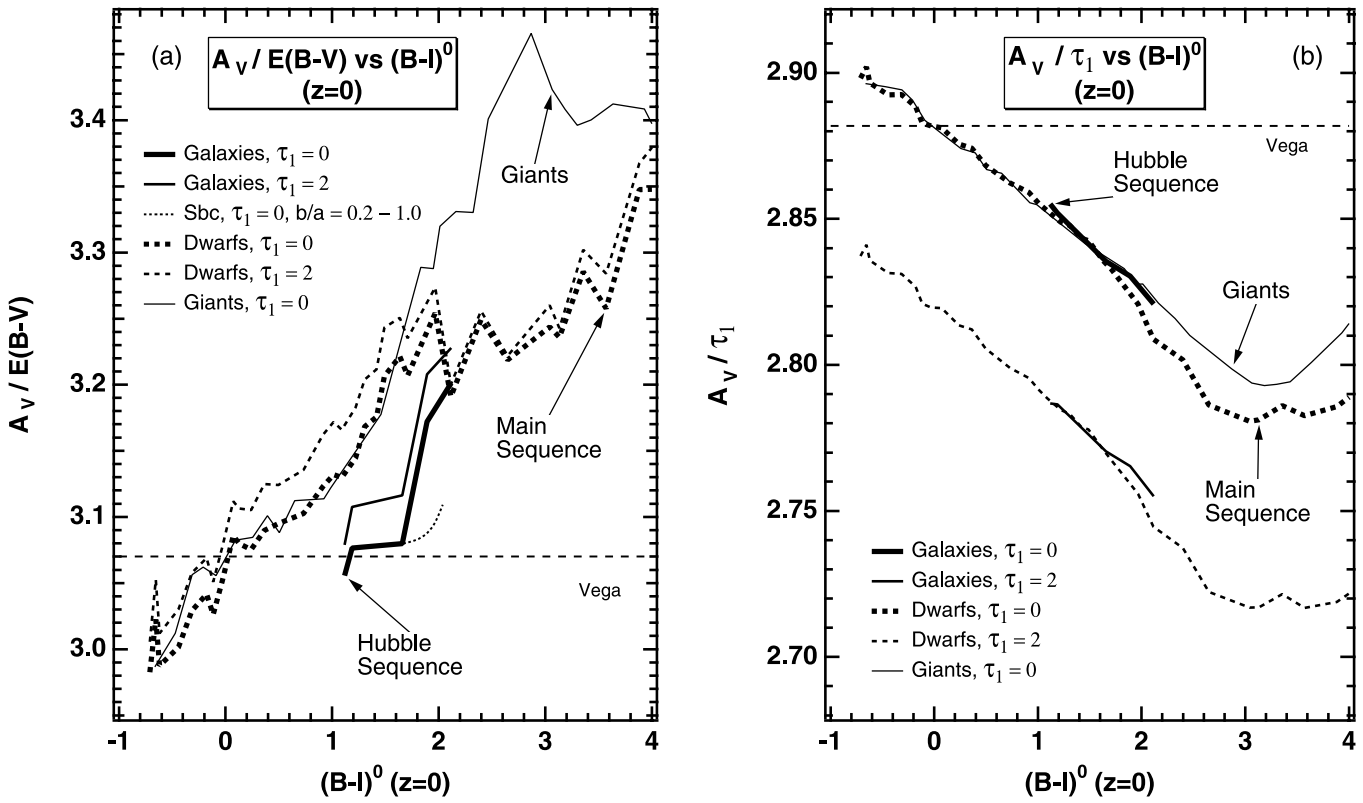

FIG. 7.—Two measures of the ratio of total to selective extinction at V for stars and galaxies as a function of the unreddened $B-I$ color in the rest frame: (*a*) $R_V = A_V/E(B-V)$; (*b*) $R'_V = A_V/\tau_1$. In both panels, trends along the HILIB main sequence (*thick dotted curves*) and the Hubble sequence (*thick solid curves*) are shown for two different choices of the optical depth of foreground dust. The trend for unobscured HILIB giants is depicted by the thinnest solid curve. For galaxies, results are presented for the original SEDs, i.e., without any adjustment for tilt. Stars are joined in order of spectral type, and galaxies in order of Hubble type. In the left panel, the thin dotted curve coming out of the Hubble sequence shows what is expected to happen to both R_V and $B-I$ as the tilt of the Sbc SED increases (to $q = 0.2$). The corresponding track in the right panel cannot be seen, since it lies right on top of the Hubble sequence. The horizontal dashed lines mark the values of R_V and R'_V for Vega.

what R'_V ought to be for the most distant supernovae discovered to date.

Figure 11 shows how R_V (*left*) and R'_V (*right*) for elliptical and irregular galaxies vary with redshift and optical depth out to $z = 1$. R_V changes quickly and drastically with redshift. For the UV-faint elliptical SED derived in this paper, it ranges from 3.5 at $z = 0.14$ to 2.6 as z approaches 1, a variation of 30%! For any galaxy, R_V can be expected to increase steadily out to $z \sim 0.1$–0.2, peaking at a value 5% to 10% higher than in the rest frame. After the peak, R_V initially declines quite rapidly, with subsequent variations being determined by the details of the SED. Note that there are redshift intervals where R_V is more sensitive to the optical depth of Galactic dust than in the rest frame.

For comparison, Figure 11 also displays trends for a starburst galaxy and for a UV-bright elliptical in the limit of zero optical depth for Galactic dust. The SED for the starburst is "Starburst 3" in the library of starburst templates created by Kinney et al. (1996). It is the average of core spectra (on the scale of the IUE aperture) for irregular and disturbed galaxies for which $E(B-V)$ due to internal dust is between 0.25 and 0.35. The wavelength resolution ranges from 6 to 10 Å. The SED for the elliptical galaxy is taken from Fukugita et al. (1995). In the optical, it is an average of the integrated spectra of elliptical and lenticular galaxies acquired by Kennicutt (1992); it is very similar to the optical portion of the elliptical SED created in this paper. However, the ultraviolet portion of the SED is determined solely by a spectrum of the core of NGC 4649 (Bertola et al. 1982), an elliptical galaxy for which $m(1650)-V$ is 1.7 mag bluer than for the galaxy (NGC 3379) defining the elliptical template derived in this paper (Rifatto et al. 1995b). Because the ultraviolet light of elliptical galaxies is more centrally concentrated than the optical, the ultraviolet component of the SED of Fukugita et al. (1995) is too bright relative to the optical (a problem afflicting most previous representations of elliptical SEDs). Nevertheless, the SED does serve to demonstrate how sensitive the z-dependences of ratios of total to selective extinction are to the shape of the ultraviolet part of elliptical spectra.

Figure 11 shows that the redshift dependences of R_V and R'_V for the starburst are very similar to what is obtained for the Im SED generated for this paper, which proves that the results for the Im SED do not suffer from the low resolution. This is, in part, because the equivalent widths of emission lines in the ultraviolet are low. On the other hand, between redshifts of 0.1 and 0.6, the trend in R_V for the UV-bright elliptical deviates from that for the UV-faint one. The strong dip centered on a redshift of 0.35 is caused by the flattening of the NGC 4649 spectrum blueward of 2900 Å. The B filter passes a lot of extra flux on its blue side, so the effective wavelength is shifted blueward, where extinction is higher. Clearly, for elliptical galaxies at redshifts beyond $\sim$0.1, it would be prudent to get a handle on the UV excess prior to deciding upon corrections for extinction.

Figure 11*b* demonstrates that changes in R'_V with redshift are considerably less than observed for R_V, although they are

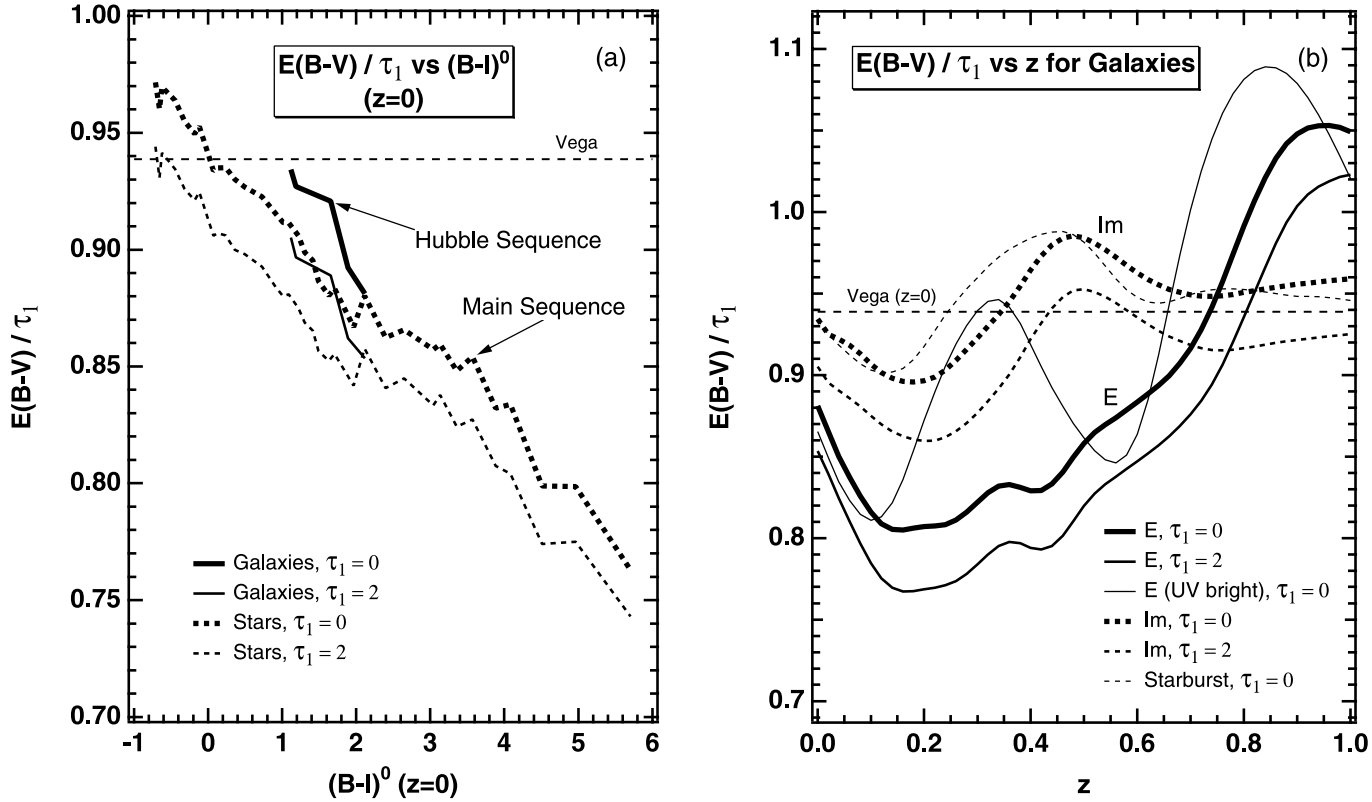

FIG. 8.—(*a*) $E(B-V)/\tau_1$ vs. intrinsic color $(B-I)^0$ for HILIB main-sequence stars and for galaxies, all at rest. (*b*) $E(B-V)/\tau_1$ vs. redshift z for elliptical and irregular galaxies. *Left*: Trends along the HILIB main sequence (*dotted curves*) and the Hubble sequence (*solid curves*) are shown for two different choices of the optical depth of foreground dust. For galaxies, results are presented for the original SEDs, i.e., without any adjustment for tilt. Stars are joined in order of spectral type, and galaxies in order of Hubble type. *Right*: Trends for the UV-faint elliptical SED (*thick solid curves*) and the irregular SED (*thick dotted curves*) derived in this paper are shown for two different choices of the optical depth of foreground dust. Also displayed are trends for a UV-bright elliptical galaxy (*thinnest solid curve*) and a starburst (*thinnest dotted curve*) in the limit of zero optical depth. The horizontal dashed lines mark the value of $E(B-V)/\tau_1$ for Vega in the rest frame.

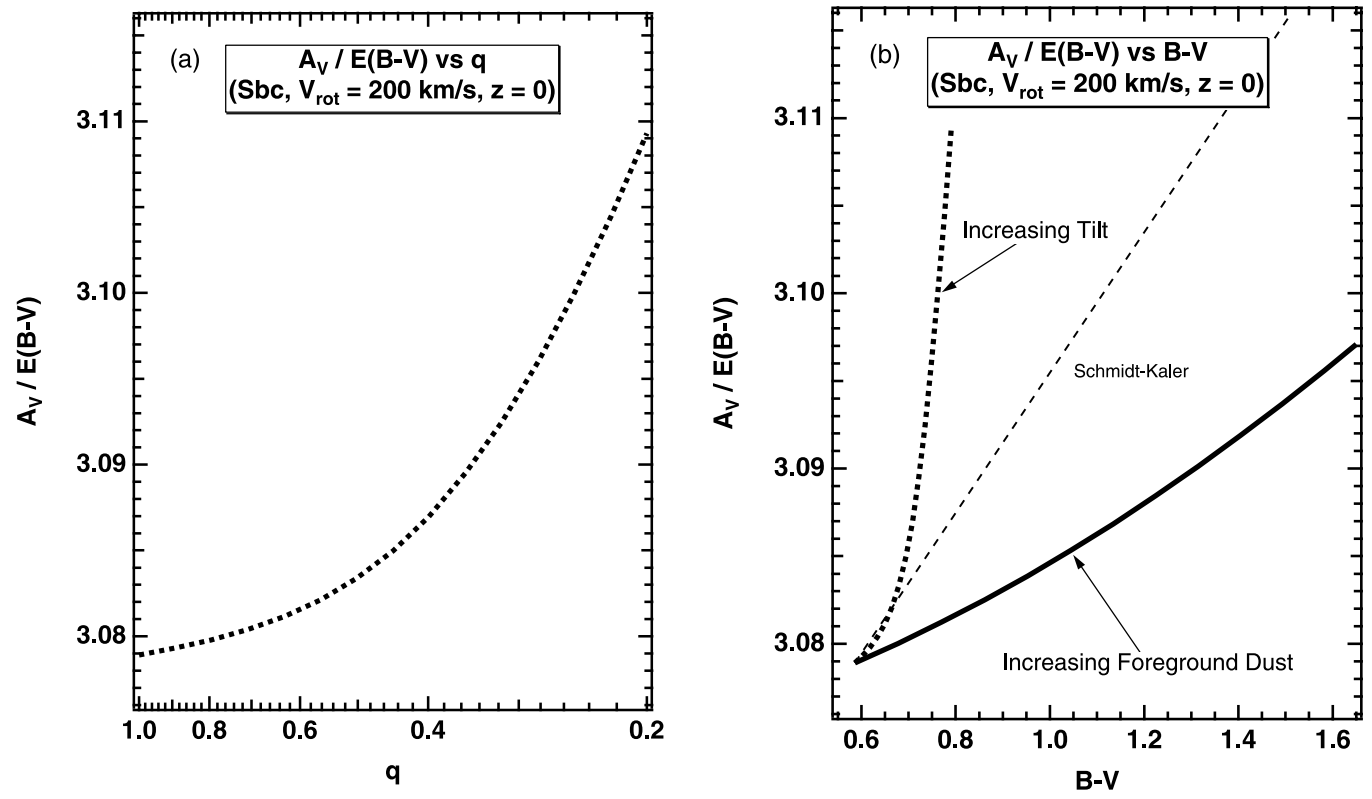

FIG. 9.—The response of $R_V = A_V/E(B-V)$ to tilt for an Sbc galaxy at rest. (*a*) R_V vs. axis ratio q (minor relative to major). (*b*) R_V vs. the apparent $B-V$ color. The dotted curves show how R_V changes with tilt. In the right panel, the solid curve shows how R_V for a face-on Sbc galaxy correlates with $B-V$ as the optical depth of foreground dust is raised. The dashed line shows the slope of the correlation specified by Schmidt-Kaler (1982) for stars (see eq. [5]).

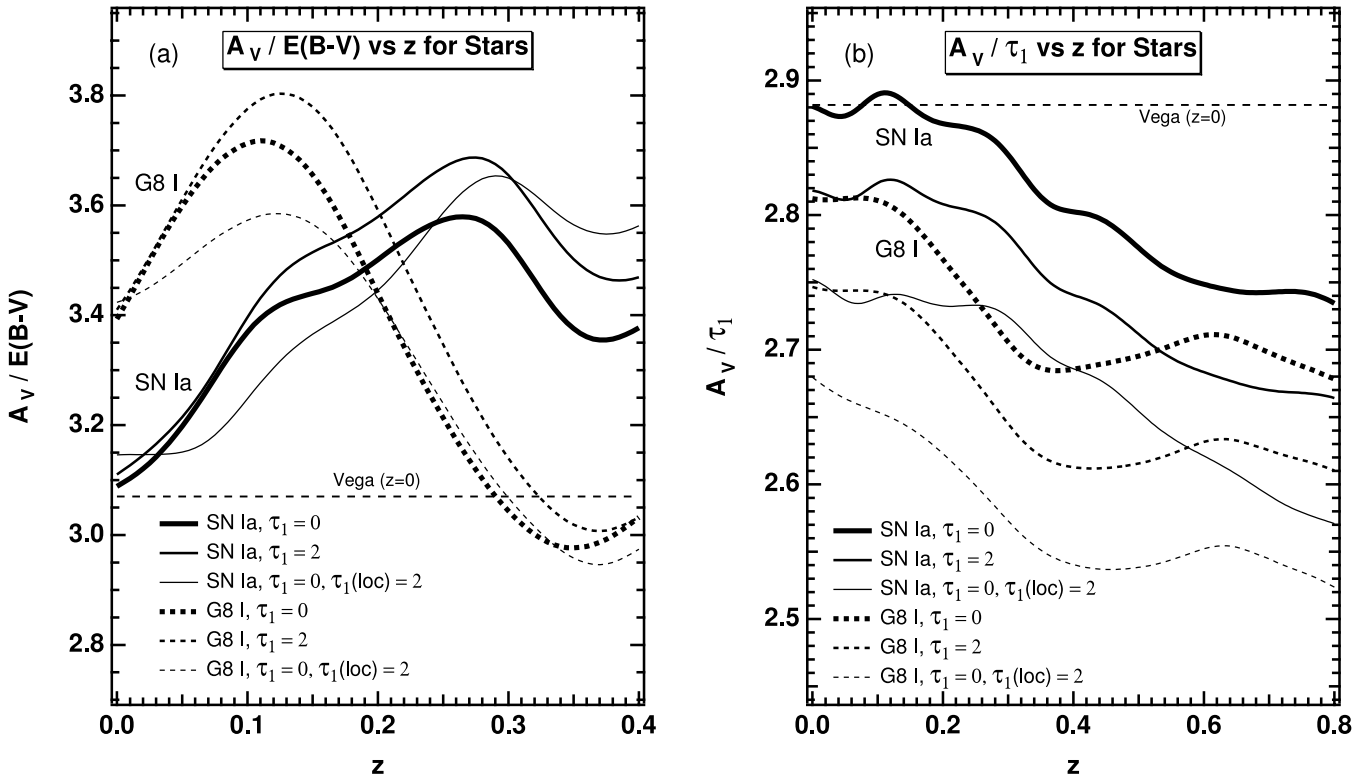

FIG. 10.—Two measures of the ratio of total to selective extinction for Galactic dust for a Type Ia supernova (3 days after maximum light, stretch 1.0) and for a luminous Cepheid (a G8 supergiant) as a function of redshift z: (*a*) $R_V = A_V/E(B-V)$; (*b*) $R'_V = A_V/\tau_1$. In both panels, trends for the supernova (*thick solid curves*) and the supergiant (*thick dotted curves*) are shown for two different choices of the optical depth of dust in the Milky Way, but assuming an optical depth for localized dust, i.e., dust in the frame of reference of the stars, equal to zero. In addition, trends are shown for stars obscured by localized dust, but not by Galactic dust (*thinnest solid and dotted curves*). For each object, differences at $z = 0$ stem from the different shapes of the SEDs upon entry into the Galactic dust layer (see text). The horizontal dashed lines mark the values of R_V and R'_V for Vega in the rest frame.

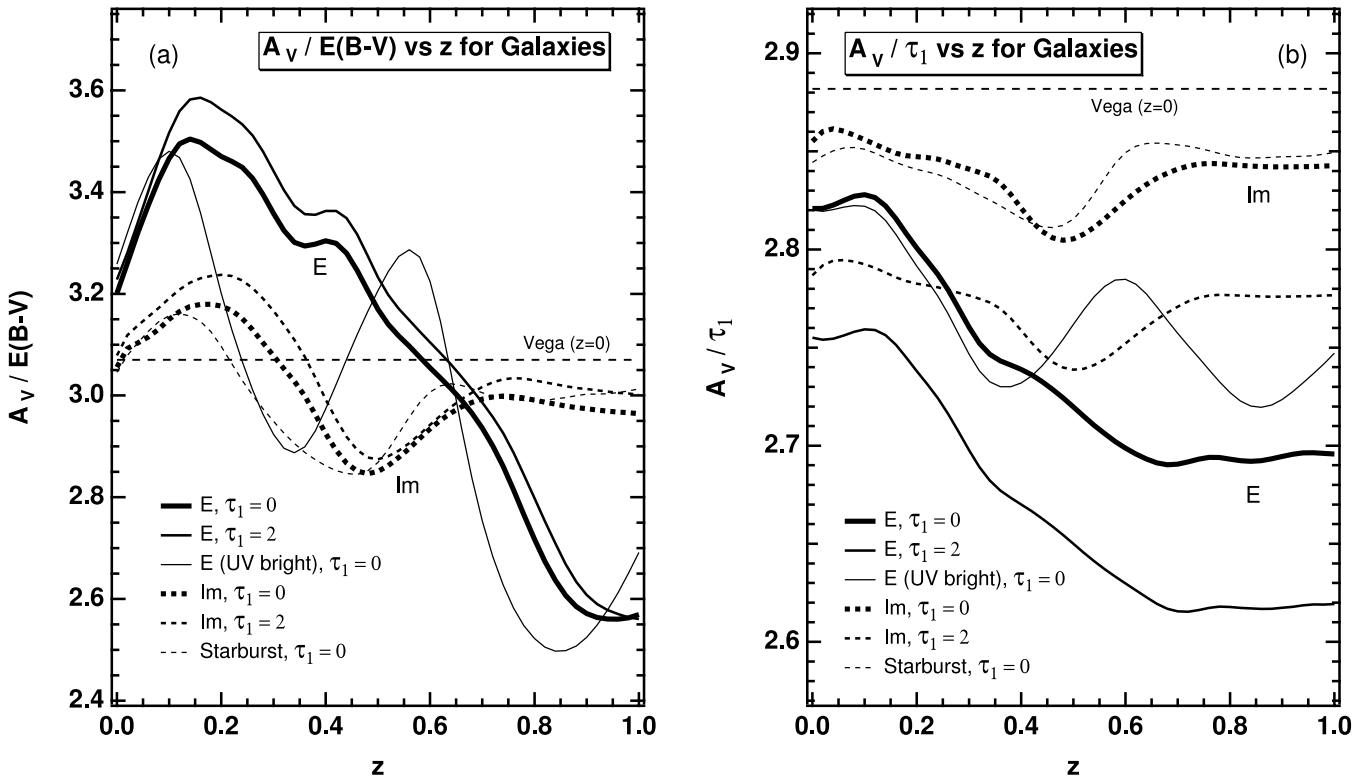

FIG. 11.—Two measures of the ratio of total to selective extinction for galaxies as a function of redshift z: (*a*) $R_V = A_V/E(B-V)$; (*b*) $R'_V = A_V/\tau_1$. In both panels, trends for the UV-faint elliptical SED (*thick solid curves*) and the irregular SED (*thick dotted curves*) derived in this paper are shown for two different choices of the optical depth of foreground dust. Also shown are trends for a UV-bright elliptical galaxy (*thinnest solid curve*) and a starburst (*thinnest dotted curve*) in the limit of zero optical depth. The horizontal dashed lines mark the values of R_V and R'_V for Vega in the rest frame.

still significant. For the UV-faint elliptical, the range of variation out to a redshift of 1.0 amounts to 5% of the value at $z = 0$, versus 30% in the case of R_V. Clearly, the primary cause of the variations in R_V is $E(B-V)$, as can be seen in Figure 8*b*.

Systematic errors in extinction estimates for galaxies might have ramifications for the study of bulk flows (Hudson 1999), because random errors, even though they may be large in comparison, average out. Thus, it is worth clarifying the significance of the results for the redshift dependence of R_V with examples involving elliptical galaxies. Consider two identical elliptical galaxies, one located at a redshift of 0.1 and the other at a redshift of 1.0. Suppose that the apparent magnitude in B has been measured for each, and that corrections for extinction must be applied to evaluate distance moduli. The challenge is to determine A_B for each from a measurement of $E(B-V)$. There are two scenarios that need to be examined:

1. Consider that $E(B-V)$ is evaluated for each galaxy by directly measuring the Mg_2 index. The Mg_2 index would give the intrinsic $B-V$ color in the rest frame, which, after applying appropriate *K*-corrections (in reverse), would be compared with the observed color to get $E(B-V)$ due to Galactic dust. It would be equivalent to *K*-correct the observed color to derive $E(B-V)$, but it is important to realize that, despite the "rest-frame" comparison, the result would apply to the *redshifted* SED. Suppose that $E(B-V)$ comes out to be 0.3 mag for both galaxies. Figure 8*b* reveals that τ_1 is 0.370 for the low-redshift galaxy, but 0.287 for the high-redshift one. Then, Figure 11*a* leads to values of R_B equal to 4.48 and 3.57, respectively. The resultant values of A_B are 1.34 and 1.07 mag for the low- and high-redshift galaxy, respectively, i.e., a difference of 0.27 mag despite starting with the same values of $E(B-V)$. If, instead, R_B is adopted to be the canonical value of 4.1, then the resultant extinctions both come out to be 1.23 mag. Despite the moderate level of reddening, the errors in the extinction that result from a cavalier treatment of R_B are significant.

2. Consider that $E(B-V)$ for each galaxy is judged from the maps of Schlegel et al. (1998). As before, suppose that $E(B-V)$ comes out to be 0.3 mag for both. In this case, the values of $E(B-V)$ apply to elliptical galaxies with $z = 0$. Figure 8*b* reveals that $\tau_1 = 0.342$ *for both galaxies*. However, values of R_B provided by Figure 11 cannot be used to derive A_B because the estimates of $E(B-V)$ do not take into account the redshifts of the galaxies. Instead, extinctions must be derived directly from τ_1. Syntheses show that the values of R'_B are 3.63 and 3.73 for the low- and high-redshift galaxies, respectively. It follows that A_B is 1.24 and 1.28 mag, respectively, a difference of only 0.04 mag due to the moderate reddening. However, if 4.1 is adopted for R_B, the extinction is systematically underestimated to be 1.23 mag.

If the ratio of total to selective extinction must be fixed, systematic errors can be minimized by restricting attention to fields for which the extinction is minimal in the wavelength bands being employed. How minimal should be judged as above for the particular range of redshift under survey. However, if wide sky coverage is paramount, such as for the local volume (i.e., out to 10 Mpc), galaxies extinguished by more than the minimum may be unavoidable. Then, it would be prudent to determine R_Λ or R'_Λ galaxy by galaxy.

4.4. *The Infrared*

Observations of heavily obscured sources are pushed into the infrared not only to improve visibility, but also to minimize corrections of observables for extinction. However, when extinction in the optical is large, extinction at *J*, *H*, or *K* is not negligible, and observables must be corrected for it. Thus, even at infrared wavelengths it is necessary to be wary of the issues raised in this paper.

Astronomers attempting to correct infrared photometry for extinction invariably employ an optical measure of reddening along with a reddening coefficient derived from some reddening law presumed to be universal in applicability. To emphasize the folly of this approach, Figure 12*a* shows for both stars and galaxies at rest how $R_H = A_H/E(B-V)$ varies with $(B-I)^0$. The *H* band is that of 2MASS. As was the case for R_V, the reddening coefficient varies dramatically with the intrinsic color of the source. Yet, as Figure 12*b* shows, $R'_H = A_H/\tau_1$ does not. The variation in R_H arises solely from the influence of effective wavelength shifts on $E(B-V)$, as displayed in Figure 8. For the same reason, R_H changes drastically with redshift, even though R'_H hardly varies at all. Thus, if $E(B-V)$ is to be employed to correct photometry at *H* for extinction, it is important to know the origins of both the reddening and the reddening law and to synchronize each to the SED of the target.

5. DISCUSSION

5.1. *What Color to Use to Derive Reddening*

If it is necessary to use broadband photometry to arrive at an estimate of reddening, there are good and bad choices for the bandpasses, depending upon the sensitivity of R'_Λ to the shape of the SED, foreground extinction, and redshift. What the above discussions make clear is that the worst possible indices of reddening are ones that involve photometry in *B*. For star-forming galaxies, bandpasses for which the response to Hα is high, such as *R* or SDSS *r*, ought to be avoided too, owing to the variability of the strength of emission.

If obscuration is not too severe, then a good alternative to $E(B-V)$ is $E(V-I)$. Photometry in both *V* and *I* can be accomplished with CCDs. Furthermore, because of the long wavelength baseline, $E(V-I)$ is more sensitive to optical depth than $E(B-V)$. For Vega in the limit of zero reddening, $E(V-I)/\tau_1 = 1.27$, whereas $E(B-V)/\tau_1 = 0.94$. For the SDSS, $E(g-i)$ would be a logical choice, although *g* is uncomfortably close to *B*. For Vega, $E(g-i)/\tau_1 = 1.75$.

Figure 13 shows how $E(V-I)/\tau_1$ and $E(g-i)/\tau_1$ depend upon the SED and Galactic extinction for both stars and galaxies. Although $E(V-I)/\tau_1$ is just as sensitive to τ_1 as $E(B-V)/\tau_1$, the ratio is much less dependent upon the intrinsic color of the source (see Fig. 8*a*). Along the main sequence, it varies by 7% versus 22% for $E(B-V)/\tau_1$. Along the Hubble sequence, $E(V-I)/\tau_1$ changes by only 2.5% versus 6% for $E(B-V)/\tau_1$. Changes in $E(g-i)/\tau_1$ are 60% larger but still roughly half as great as those observed for $E(B-V)/\tau_1$.

Figure 14 shows for galaxies how $E(V-I)/\tau_1$ and $E(g-i)/\tau_1$ depend upon redshift and Galactic extinction. For the elliptical, both $E(V-I)/\tau_1$ and $E(g-i)/\tau_1$ vary by about 10% out to $z = 1$. In comparison, $E(B-V)/\tau_1$ changes by 28% over the same range in redshift (see Fig. 8*b*).

If extinction is severe, a more readily accessible index of reddening would be $J-K_s$ (2MASS). Figure 15 shows how $E(J-K_s)/\tau_1$ depends upon the SED, Galactic extinction, and redshift. Along the main sequence, the range of variation is only 5%. Along the Hubble sequence, the ratio varies by only 0.5%. Out to a redshift of unity, the ratio for elliptical galaxies varies remarkably little. In the case of irregular galaxies, it spans a range that is only 2.5% of the value in the rest frame.

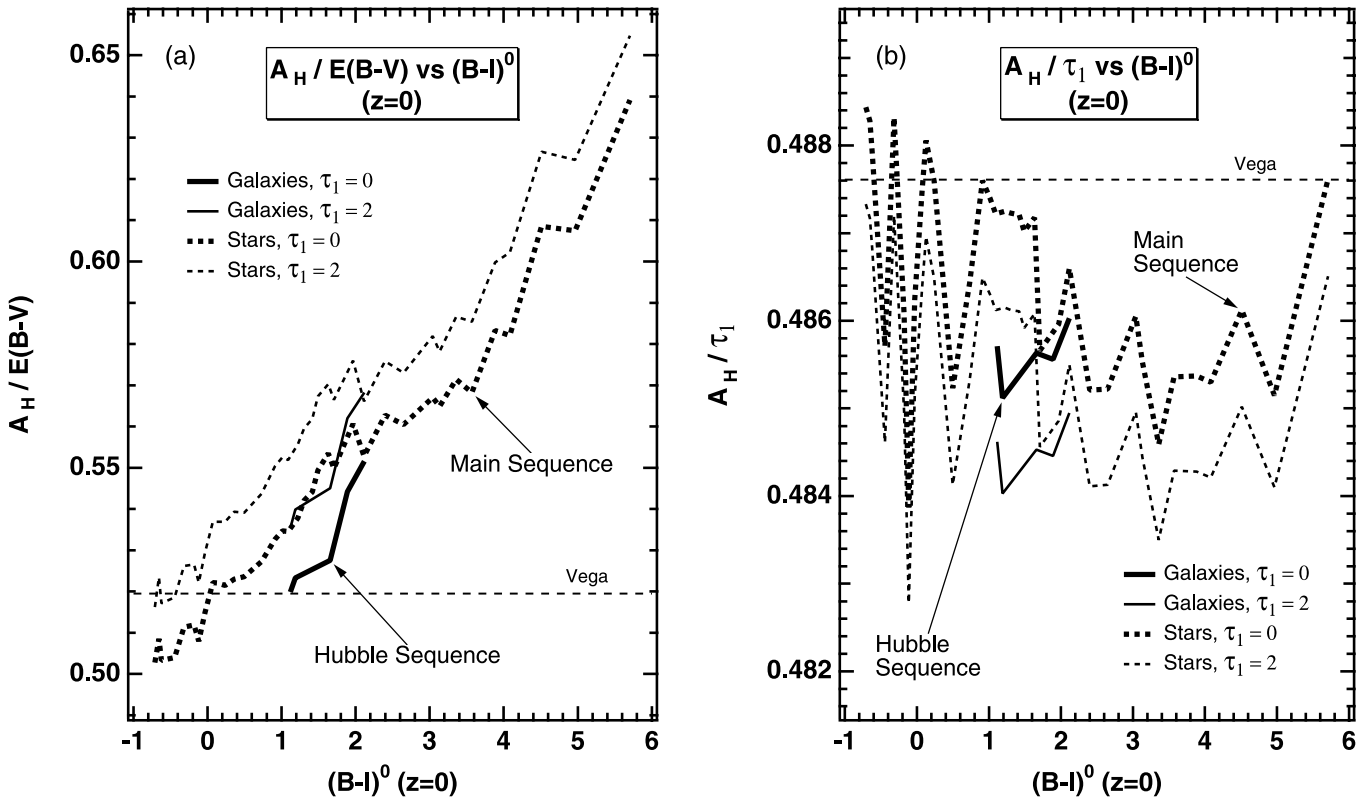

FIG. 12.—Two measures of the ratio of total to selective extinction for 2MASS H for stars and galaxies as a function of the unreddened $B-I$ color in the rest frame: (*a*) $R_H = A_H/E(B-V)$; (*b*) $R'_H = A_H/\tau_1$. In both panels, trends along the HILIB main sequence (*dotted curves*) and the Hubble sequence (*solid curves*) are shown for two different choices of the optical depth of foreground dust. For galaxies, results are presented for the original SEDs, i.e., without any adjustment for tilt. Stars are joined in order of spectral type, and galaxies in order of Hubble type. The horizontal dashed lines mark the values of R_H and R'_H for Vega. Even though R'_H hardly changes with color, R_H varies substantially owing to the influence of effective wavelength shifts on $E(B-V)$.

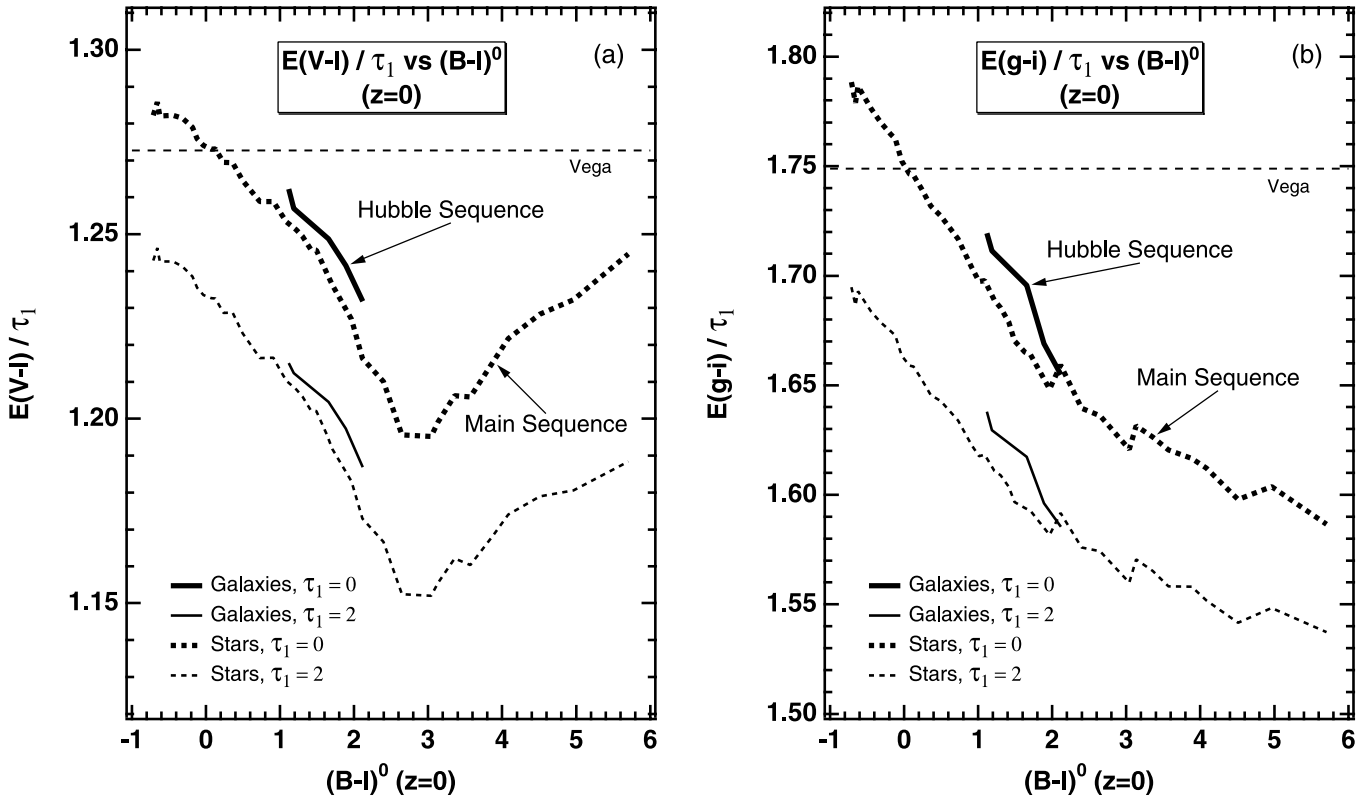

FIG. 13.—(*a*) $E(V-I)/\tau_1$ and (*b*) $E(g-i)/\tau_1$ vs. intrinsic color $(B-I)^0$ for stars and galaxies at rest ($z = 0$). Dotted curves connect results for HILIB main-sequence SEDs in order of spectral type. Solid curves sequence results for the galaxy SEDs generated for this paper in order of Hubble stage. Results are shown for two different choices of the optical depth of Galactic dust. The horizontal dashed lines mark values for Vega.

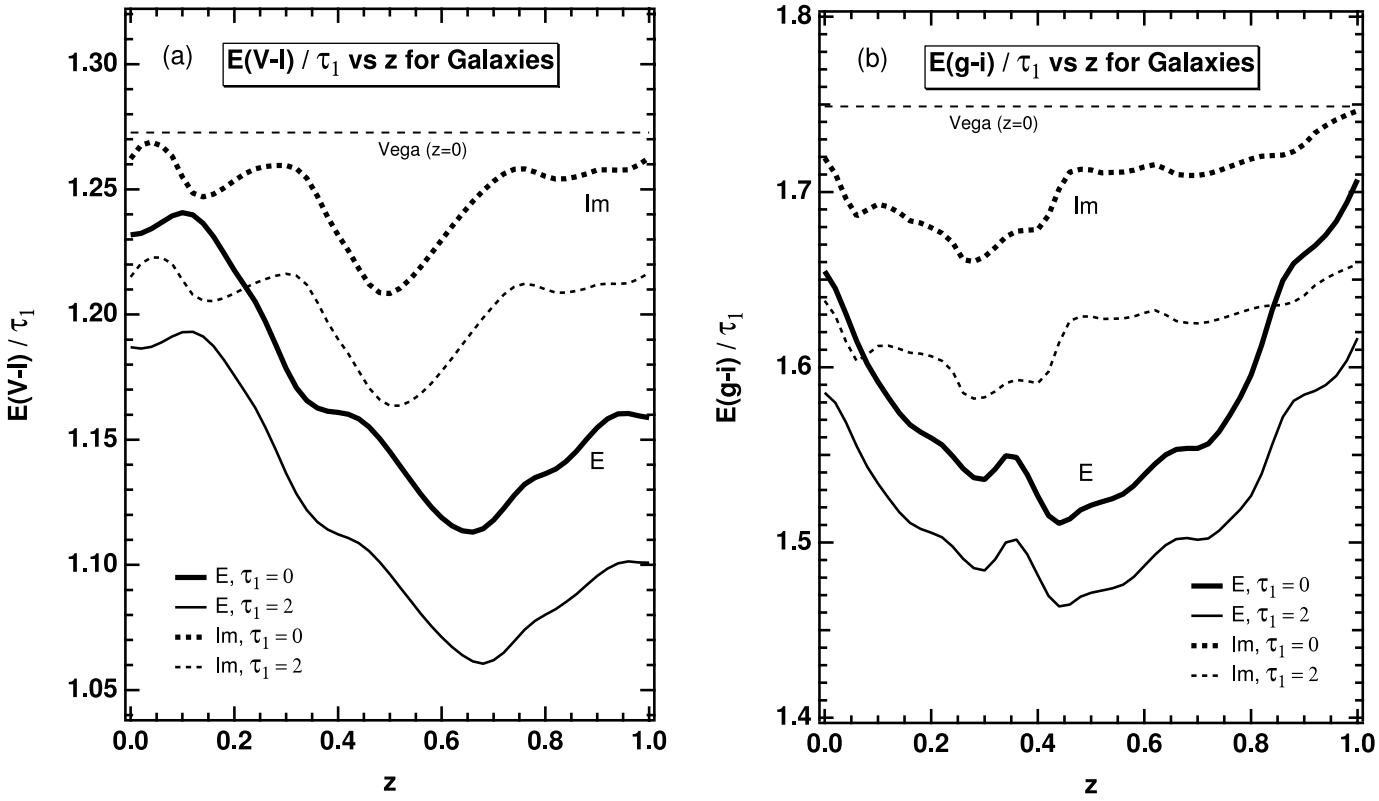

FIG. 14.—(*a*) $E(V-I)/\tau_1$ and (*b*) $E(g-i)/\tau_1$ vs. redshift z for elliptical (UV-faint) and irregular galaxies. Results are shown for two different choices of the optical depth of Galactic dust. The horizontal dashed lines give results for Vega in the rest frame.

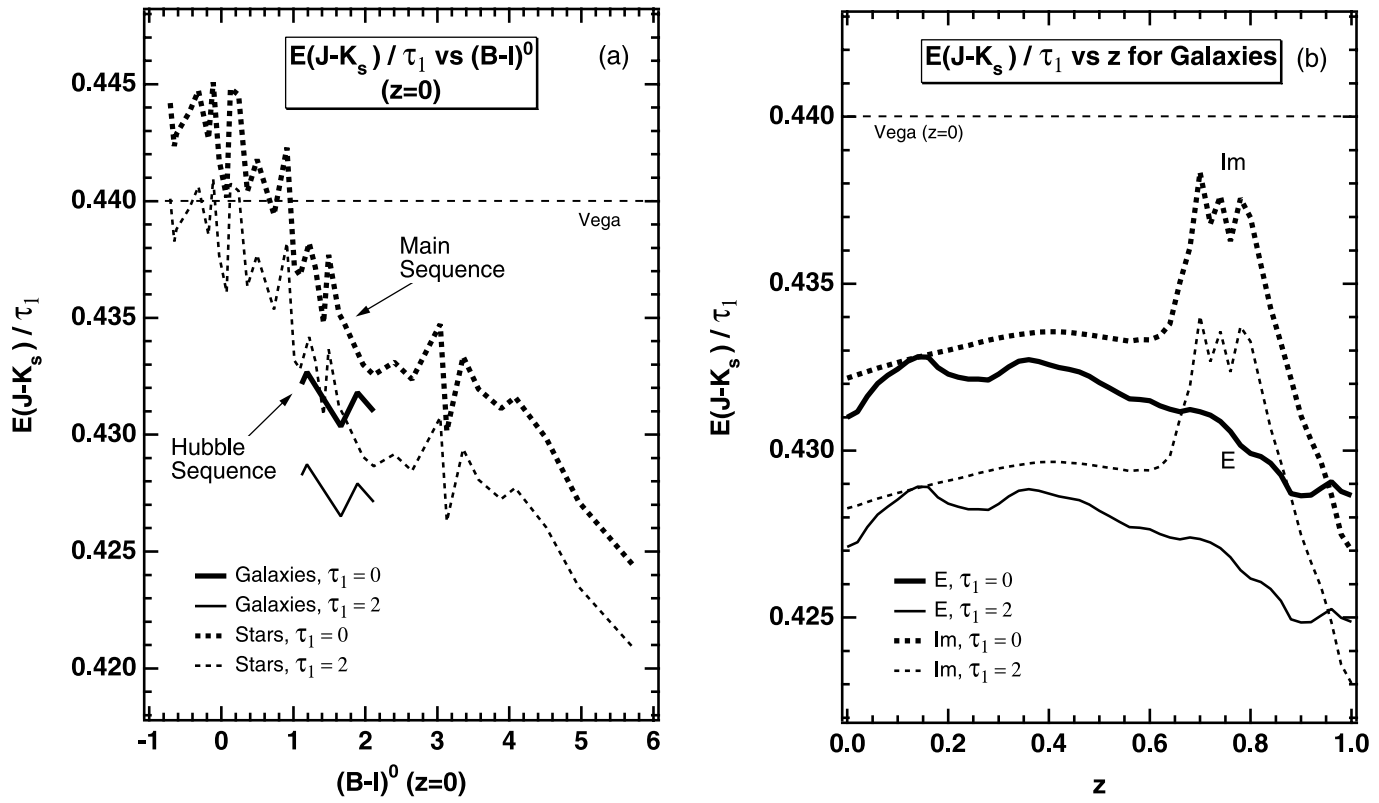

FIG. 15.—(*a*) $E(J-K_s)/\tau_1$ vs. intrinsic color $(B-I)^0$ for stars and galaxies at rest. (*b*) $E(J-K_s)/\tau_1$ vs. redshift z for elliptical (UV-faint) and irregular galaxies. *Left*: Trends along the HILIB main sequence (*dotted curves*) and the Hubble sequence (*solid curves*) are shown for two different choices of the optical depth of foreground dust. For galaxies, results are presented for the original SEDs, i.e., without any adjustment for tilt. Stars are joined in order of spectral type, and galaxies in order of Hubble type. *Right*: Trends for the UV-faint elliptical galaxy SED (*solid curves*) and the irregular galaxy SED (*dotted curves*) derived in this paper are shown for two different choices of the optical depth of foreground dust. The horizontal dashed lines mark the value of $E(J-K_s)/\tau_1$ for Vega in the rest frame.

Unfortunately, the sensitivity of $E(J-K_s)$ to optical depth is half that of $E(B-V)$, and a third that of $E(V-I)$.

5.2. *Recommendations for Deriving Extinction from Reddening*

Paths to estimating the effects of Galactic dust upon the light of celestial bodies are invariably guided by color indices founded upon broadband photometry. A color index may apply specifically to a source, as would be the case if it were derived by comparing the intrinsic color with the apparent color, or to objects completely different from the source, such as stellar probes of extinction located within a galaxy or the OB stars used to construct the reddening law. The key to deriving extinction reliably is to convert the measure of reddening into the optical depth of dust actually causing it. Knowing the optical depth at a fiducial wavelength, it is possible to derive the extinction in any bandpass for any source without having to worry about how the reddening was judged in the first place. Therefore, to determine the Galactic extinction A_{Λ_3} in bandpass Λ_3 starting from a color index $E(\Lambda_1-\Lambda_2)$ derived from photometry in bandpasses Λ_1 and Λ_2, it is recommended that the following steps be taken:

1. Determine the nature of the source used to estimate $E(\Lambda_1-\Lambda_2)$. If it is a star, note the spectral type and luminosity class and guess the optical depth due to *localized dust*, that is, the optical depth of dust in the immediate vicinity of the star as it would be perceived in a frame of reference comoving with the star. If it is a galaxy, note the Hubble type. If it is a spiral galaxy, note the axis ratio and the rotational velocity. In all cases, note the redshift too.
2. Guess $\tau_1^{\rm gal}$, the optical depth at 1 μm due to Galactic dust. One possibility is to guess $E(B-V)$ and then set $\tau_1^{\rm gal}$ equal to it. The guess need not be very good, because it is only used to extinguish the SED of the reddening probe for the purpose of evaluating ratios of total to selective extinction, which are not very sensitive to $\tau_1^{\rm gal}$.
3. Synthesize $R'_{\Lambda_1} = A_{\Lambda_1}/\tau_1$ and $R'_{\Lambda_2} = A_{\Lambda_2}/\tau_1$ using the SED for the source from which $E(\Lambda_1-\Lambda_2)$ was derived. In the case of a star, the SED should be adjusted first for localized dust and for redshift. In the case of the galaxy, the SED should be adjusted to the right tilt (via the axis ratio and rotational velocity) and redshift. Then, whatever the case, the SED should be extinguished using the estimate for $\tau_1^{\rm gal}$ in conjunction with a monochromatic law of reddening that is known to deliver a value of $R_V = A_V/E(B-V)$ characteristic of the obscuring medium when applied to the spectrum of a reference source for which this ratio is known.
4. Compute $\tau_1^{\rm gal}$ by dividing $E(\Lambda_1-\Lambda_2)$, corrected as necessary for localized reddening, by $R'_{\Lambda_1} - R'_{\Lambda_2}$.
5. Iterate through steps 3 and 4 until $\tau_1^{\rm gal}$ converges.
6. Determine the nature of the source for which the extinction is required. If it is a star, note the spectral type and luminosity class and guess the optical depth due to localized dust. If it is a galaxy, note the Hubble type. If it is a spiral galaxy, note the axis ratio and the rotational velocity. In all cases, note the redshift too.
7. Synthesize $R'_{\Lambda_3} = A_{\Lambda_3}/\tau_1$ using the SED for the source for which the extinction is needed. In the case of a star, the SED should be adjusted first for localized dust and for redshift. In the case of a galaxy, the SED should be adjusted to the right tilt (via the axis ratio and rotational velocity) and redshift. Then, whatever the case, the SED should be extinguished using the derived value of $\tau_1^{\rm gal}$ along with the monochromatic law of reddening.
8. Compute A_{Λ_3} by multiplying R'_{Λ_3} by $\tau_1^{\rm gal}$.

In the case of nebulae, the first six steps above can be avoided. Monochromatic indices of reddening, such as the flux ratio $F(\mathrm{H}\alpha)/F(\mathrm{H}\beta)$, are available. If a truly monochromatic reddening law is employed (including being normalized to τ_1), then $\tau_1^{\rm gal}$ can be estimated directly.

In the case of a star, a color index reflects the combined effect of dust that is widespread in the Milky Way and localized dust in the frame of reference of the star, such as in another galaxy. It is often the case that the optical depth due to dust in the Milky Way is known, say, from an all-sky map, but the optical depth due to localized dust moving with the host is not. How to determine the right corrections for Galactic and localized dust in this case is described with the aid of an example in the next section.

5.3. *Applications*

To clarify some of the concepts of this paper, it is useful to go through two examples. Of particular interest are Cepheid distances, owing to their pivotal role in work on the extragalactic distance scale. Distances to M31 derived from three different fields are examined first, to reevaluate the sensitivity of the period-luminosity (P-L) relation to metallicity. Second, the Cepheid distance to NGC 4258 is redetermined to see how much of the discrepancy with respect to the maser result might be due to the method of handling extinction. Although the Cepheids are not highly extinguished in either galaxy, they serve to illustrate how the work described in this paper might be brought to bear upon real problems.

Using the Canada-France-Hawaii Telescope, Freedman & Madore (1990) observed Cepheids in three fields in M31 with metallicities ranging from $\sim$0.3 to $\sim$1.7 times solar. By comparing measurements in different bandpasses, they were able to determine reddenings and distances simultaneously. In order of decreasing metallicity (increasing radius), the observations in V and I (which are most relevant to the *HST* key project on H_0) yielded extinctions in V equal to 0.61, 0.84, and 0.00 mag, which led to distance moduli of 24.32, 24.33, and 24.58, with an average of 24.41 (assuming an LMC distance modulus of 18.50). The reddening law employed was that of Cardelli et al. (1989). Notably, the highest distance was measured for the least extinguished field.

Based upon the periods of the observed Cepheids, it is not unreasonable to approximate their spectra to be like that of an F8 supergiant. The apparent distance moduli in V and I yield values of $E(V-I)$ equal to 0.24, 0.33, and -0.01. Approximating the Cepheids to be at rest with respect to the Sun, the corresponding values of τ_1 are 0.193, 0.266, and 0. The resulting values of A_V/τ_1 give A_V equal to 0.548, 0.754, and 0, the first two now lower than previously estimated. In turn, the corrected distance moduli become 24.38, 24.42, and 24.58, with an average of 24.46 (for an LMC distance modulus of 18.50). The results for the extinguished fields are now significantly less discrepant from that for the unextinguished one, which confirms the contention that the P-L relation does not depend strongly on metallicity. Note that the mean distance modulus has risen by 0.05 mag. However, a similar analysis of LMC Cepheids would be necessary to determine if there is actually a change differentially.

For NGC 4258, from *HST* observations of Cepheids in V and I, Newman et al. (2001) derived the extinction to be 0.50 mag in V, from which a corrected distance modulus of 29.40 was determined (before accounting for metallicity and again assuming an LMC distance modulus of 18.50). The metallicity-corrected

distance is 0.17 dex (1.2 σ) higher than the geometric distance derived from a study of the orbital motions of masers in the core of the galaxy (Herrnstein et al. 1999).

The *apparent* Cepheid distance moduli in V and I are 29.90 and 29.69, respectively. Thus, the apparent reddening is $E(V-I) = 0.21$. According to Schlegel et al. (1998), the Galactic reddening in the direction of NGC 4258 is only $E(B-V) = 0.016$. Thus, most of the reddening is *localized* in origin. Although the redshift of the galaxy is only $z = 0.0015$, and might just as well be regarded as zero, it is useful to see how a rigorous examination of extinction should proceed. To correct the distance moduli for extinction, it is necessary to do the following:

1. Make an initial guess for the optical depth of localized dust (the optical depth of dust for an observer outside of the Milky Way comoving with NGC 4258), say, from the difference between the total and Galactic color excesses.
2. Following the steps outlined in § 5.2, determine the optical depth of Galactic dust from the color excess provided by Schlegel et al. (1998) using the SED of an unobscured elliptical galaxy at rest.
3. Determine the extinction coefficients for Galactic dust using the SED of an appropriately redshifted Cepheid extinguished by the localized dust.
4. Correct the apparent distance moduli for Galactic dust using the estimate of the optical depth of Galactic dust.
5. *K*-correct the distance moduli using the SED for an appropriately redshifted Cepheid extinguished by the localized dust.
6. Compute the color excess from the corrected distance moduli and reevaluate the optical depth of localized dust (now working in the frame of the Cepheids).
7. Go back to step 3, iterating until the optical depth of localized dust converges.
8. Repeat steps 3, 4, and 5 to derive distance moduli corrected for Galactic dust and redshift.
9. Determine extinction coefficients in the frame of the Cepheid, that is, for a Cepheid at rest obscured by the optical depth of localized dust.
10. Correct the distance moduli derived in step 8 for localized dust.

The estimate of the Galactic reddening is founded upon the colors of elliptical galaxies at rest. Using the elliptical SED, the optical depth due to Galactic dust comes out to be $\tau_1^{\rm gal} = 0.018$. Approximating the Cepheids to have spectra like F8 supergiants, the optical depth of localized dust converges to $\tau_1^{\rm loc} = 0.149$. The resulting values of the Galactic and localized extinction in V are 0.052 and 0.423 mag, respectively. The *K*-correction is +0.001 in *V*. Consequently, the distance modulus corrected for everything but metallicity is 29.424. The result is 0.024 mag higher than estimated by Newman et al. (2001). The actual shift might be slightly less if the Cepheids in the LMC are analyzed in a similar manner. However, the distance remains discrepant with that derived from masers.

6. CONCLUSIONS

Permeating astronomy is the need to correct observables for obscuration by Galactic dust. Techniques for gauging extinction are predominantly differential, which means that a value of the ratio of total to selective extinction (R) must be adopted to arrive at an estimate of the extinction from a measurement of the reddening. Unfortunately, most measurements of brightness and reddening are founded upon observations through broadband filters. The effective wavelengths are known to depend upon the SED being transmitted, which is determined by the intrinsic nature of the source, its redshift, and its extinction both by dust in the Milky Way and by dust localized in the frame of reference of the source. Thus, the shape of the apparent SED determines by how much its broadband magnitudes are extinguished by a given layer of dust. In addition, an estimate of the reddening of a target is sensitive to the apparent SED of the *probe* of reddening, which is usually not the same as that of the target. Furthermore, the value of R defined by a reddening law may be sensitive to the SEDs of the sources used to derive the law. All three factors have a bearing on how an estimate of reddening is converted into an estimate of extinction. Usually only the first is considered, and then only in the context of correcting *UBV* photometry of stars. For extragalactic sources, there has been hardly any examination of these issues. In any study of extinction-dependent quantities, it is prudent to account properly for changes in R arising from shifts in effective wavelengths in order to minimize the potential for systematic errors.

In this paper, a framework has been developed for correcting any kind of photometry for extinction in a manner that fully compensates for shifts in effective wavelengths. What is important is that any measure of reddening for a target first be converted into an optical depth at some standard wavelength with the aid of a monochromatic law of reddening. This step is needed to remove the effect of any bandpass shifts upon the reddening estimate by the source or sources used to derive it. The optical depth can be derived iteratively from a color excess with the aid of a SED approximating that of the reddening probe. With knowledge of an optical depth, it then becomes possible to arrive at an estimate of extinction that is appropriately tuned to the target for any bandpass.

The recommended standard wavelength is 1 μm because reddening laws are not very sensitive to environment in the near-infrared and because the optical depth at 1 μm is numerically close to $E(B-V)$. The recommended reddening law is the version of the monochromatic law provided by Fitzpatrick (1999), renormalized to the optical depth at 1 μm, which delivers $A_V/E(B-V) = 3.07$ when integrated over the spectrum of Vega. The chosen value of $A_V/E(B-V)$ is what is observed for stars of zero color in the limit of zero extinction by a variety of different techniques and typifies the dust in the diffuse interstellar medium, which is largely responsible for obscuring sources whose light traverses a long path through the Milky Way.

To study R for galaxies, *integrated* SEDs spanning the space ultraviolet to 3.8 μm were created for a range of Hubble types. SEDs for Hubble types E, Sab, Sbc, and Im each were constructed from data for a single representative galaxy, and the SED for Scd from data for two representative galaxies of comparable inclination. This way, the SEDs were specific to well-defined tilts, thereby making adjustments to derive SEDs for different inclinations possible. Observations of broadband colors as a function of axis ratio were fitted with a dust model employing the recommended reddening law to arrive at a function suitable for transforming the SEDs of the disk galaxies.

Along the main sequence, $A_V/E(B-V)$ varies by 23%, with the value for most spectral types being higher than the canonical value of 3.1. Later than K2, the ratio becomes quite sensitive to the luminosity class too, with values for evolved stars deviating by up to 17% from those for dwarfs. Along the Hubble sequence, $A_V/E(B-V)$ varies by 5%. For elliptical

galaxies, the ratio is 3.20, which is comparable to that of main-sequence stars of the same color, but 4% less than the value found for giants. At a given color, a star-forming galaxy has a value of $A_V/E(B-V)$ up to 5% lower than that for a main-sequence star. Primarily, this is because the mixture of stellar populations in the galaxy leads to a different distribution of flux across the B band. The ratio is not very sensitive to the level of foreground extinction. For galaxies, $A_V/E(B-V)$ changes much faster with tilt than with optical depth, but the range of variation from face-on to near edge-on amounts to only 1%. For both stars and galaxies, $A_V/E(B-V)$ varies dramatically with redshift, by 16% and 22% for a Type Ia supernova and luminous Cepheid, respectively, out to $z = 0.4$, and by 30% in the case of elliptical galaxies out to $z = 1$. For elliptical galaxies, the behavior with redshift is strongly dependent upon the UV excess. Even in the infrared, it is necessary to be wary of effective wavelength shifts, because extinction corrections are usually tied to optical measures of reddening. For example, $A_H/E(B-V)$ depends strongly on both intrinsic color and redshift but solely because of the sensitivity of $E(B-V)$ to these parameters.

Most of the problems with $A_V/E(B-V)$ arise from variations in the effective wavelength of the B band with respect to the V band. In evaluating the reddening of a source, it is recommended that an index be employed that avoids B. A good choice is $E(V-I)$, which is less sensitive to the shape of the apparent SED and to redshift. The long wavelength span actually makes $E(V-I)$ more sensitive to optical depth than $E(B-V)$. Another advantage is that the color has been measured widely for both stars and galaxies. For the most heavily reddened objects, $E(J-K_s)$ may be a useful diagnostic of extinction, although it is 3 times less sensitive to optical depth than $E(V-I)$.

To determine the extinction of a source from an estimate of reddening, the optical depth at 1 μm should be computed first, using a SED like that of the probe of reddening, appropriately extinguished and redshifted. Then, the optical depth can be used to evaluate the extinction in any bandpass with the aid of a SED similar to that of the source, appropriately extinguished and redshifted. It is important that a monochromatic law of reddening be employed in these processes that delivers a ratio of total to selective extinction characteristic of the obscuring medium when it is applied to the spectrum of a reference source, such as Vega, for which the ratio is known.

To make it easy for astronomers to follow the recommended methodologies for estimating extinction from reddening (especially, the multistep processes described in §§ 5.2 and 5.3), the software developed for this paper has been interfaced to a Web site. The York Extinction Solver (YES) enables the determination of an appropriate estimate of either the Galactic or localized extinction of a star, star cluster, galaxy, or galaxy nucleus from any differential measure of extinction. Colors and K-corrections are computed simultaneously to facilitate a fully self-consistent analysis of any given source. To place nebular diagnostics of extinction on the same footing, the Spreadsheet Nebular Analysis Package (Krawchuk et al. 1997) has been updated to include the same reddening law (Fitzpatrick 1999) and to quantify extinction in terms of the optical depth at 1 μm.

The author is grateful to the Natural Sciences and Engineering Research Council of Canada for its continuing support. Special thanks are conveyed to M.-H. Armour, who assisted early on with the exploration of reddening laws and techniques of integration. E. Fitzpatrick provided valuable advice on reddening and kindly made available his IDL script for computing monochromatic reddening laws, from which it was possible to develop code in Fortran and in Visual Basic to duplicate his laws. K. Shimasaku was particularly helpful in discussions about the construction of galaxy SEDs and also in making available the response curves used in Fukugita et al. (1995). The author is especially thankful to M. Bessell for invaluable information and advice about filter response curves and for supplying a copy of the model spectrum of Vega used in Bessell et al. (1998). The author is also grateful to A. Rifatto for clarifying issues related to integrated ultraviolet magnitudes, and to C. Impey for explaining the photometric system behind his measurements at L'. Special thanks are owed to C. Liu and R. Jansen for providing integrated spectra of Scd galaxies in advance of publication, and to F. Mannucci for making available his uncorrected infrared spectra of NGC 3379. The author is grateful to P. Marcum for supplying tables of Astro-1 UV photometry in advance of publication (see Marcum et al. 2001). Thanks are given to R. Fingerhut for reading over the manuscript in advance of submission. Finally, the author is indebted to Drs. P. Barnes, M. Doherty, J. Marshall, M. Ng, and most of all, S. McCall, for their heroic efforts to prevent him from being buried in dust before this work was completed.

REFERENCES

Baggett, S., Casertano, S., & Wiggs, M. 1997 May 30, accessed 2001 July from ftp://ftp.stsci.edu/cdbs/cdbs8/synphot_tables
Bertola, F., Capaccioli, M., & Oke, J. B. 1982, ApJ, 254, 494
Bessell, M. S. 1990, PASP, 102, 1181
Bessell, M. S., & Brett, J. M. 1988, PASP, 100, 1134
Bessell, M. S., Castelli, F., & Plez, B. 1998, A&A, 333, 231
Binney, J., & Merrifield, M. 1998, Galactic Astronomy (Princeton: Princeton Univ. Press)
Boselli, A., & Gavazzi, G. 1994, A&A, 283, 12
Blanco, V. M. 1956, ApJ, 123, 64
Bosma, A., Goss, W. M., & Allen, R. J. 1981, A&A, 93, 106
Bottinelli, L., Gouguenheim, L., Paturel, G., & de Vaucouleurs, G. 1983, A&A, 118, 4
Burstein, D., & Heiles, C. 1982, AJ, 87, 1165
———. 1984, ApJS, 54, 33
Buta, R. J., & Williams, K. L. 1995, AJ, 109, 543
Cardelli, J. A., Clayton, G. C., & Mathis, J. S. 1989, ApJ, 345, 245
Castelli, F., & Kurucz, R. L. 1994, A&A, 281, 817
Cline, A. K. 1989, FITPACK Library, Guide to Available Mathematical Software (GAMS), http://gams.nist.gov
Code, A. D., & Welch, G. A. 1982, ApJ, 256, 1
Cohen, M., Wheaton, Wm. A., & McGeath, S. T. 2003, AJ, 126, 1090
Coleman, G. D., Wu, C.-C., & Weedman, D. W. 1980, ApJS, 43, 393
Crawford, D. L., & Barnes, J. V. 1970, AJ, 75, 978
Cutri, R. M., et al. 2003, Explanatory Supplement to the 2MASS All Sky Data Release (Pasadena: Caltech), http://www.ipac.caltech.edu/2mass/releases/allsky/doc
de Vaucouleurs, G., de Vaucouleurs, A., Corwin, H. G., Jr., Buta, R. J., Paturel, G., & Fouqué, P. 1991, Third Reference Catalogue of Bright Galaxies (New York: Springer)
Fingerhut, R. L. 2002, M.Sc. thesis, York Univ.
Fingerhut, R. L., McCall, M. L., De Robertis, M., Kingsburgh, R. L., Kolmjenovic, M., Lee, H., & Buta, R. J. 2003, ApJ, 587, 672
Fitzpatrick, E. L. 1999a, PASP, 111, 63
Freedman, W. L., & Madore, B. F. 1990, ApJ, 365, 186
Fukugita, M., Shimasaku, K., & Ichikawa, T. 1995, PASP, 107, 945
Golay, M. 1974, Introduction to Astronomical Photometry (Dordrecht: Reidel)
Hanbury Brown, R., Davis, J., & Allen, L. R. 1974, MNRAS, 167, 121
Herrnstein, J. R., et al. 1999, Nature, 400, 539

Holtzman, J. A., Burrows, C. J., Casertano, S., Hester, J. J., Trauger, J. T., Watson, A. M., & Worthey, G. 1995, PASP, 107, 1065
Hudson, M. J. 1999, PASP, 111, 57
Hunter, D. A., van Woerden, H., & Gallagher, J. S. 1999, AJ, 118, 2184
Hunter, D. A., Wilcots, E. M., van Woerden, H., Gallagher, J. S., & Kohle, S. 1998, ApJ, 495, L47
Impey, C. D., Wynn-Williams, C. G., & Becklin, E. E. 1986, ApJ, 309, 572
Jansen, R. A., Fabricant, D., Franx, M., & Caldwell, N. 2000, ApJS, 126, 331
Jarrett, T. H., Chester, T., Cutri, R., Schneider, S. E., & Huchra, J. P. 2003, AJ, 125, 525
Johnson, H. L. 1965, ApJ, 141, 923
Kennicutt, R. C., Jr. 1992, ApJS, 79, 255
Kent, S. M. 1985, PASP, 97, 165
Kinney, A. L., Calzetti, D., Bohlin, R. C., McQuade, K., Storchi-Bergmann, T., & Schmitt, H. R. 1996, ApJ, 467, 38
Krawchuk, C. A. P., McCall, M. L., Kolmjenovic, M., Kingsburgh, R., Richer, M., & Stevenson, C. 1997, in IAU Symp. 180, Planetary Nebulae, ed. H. J. Habing and H. J. G. L. M. Lamers (Dordrecht: Kluwer), 116
Le Borgne, J.-F., et al. 2003, A&A, 402, 433
Leitherer, C., et al. 1996, PASP, 108, 996
Liu, C. T., Knezek, P. M., Worthey, G., & Scott, J. E. 1999, BAAS, 31, 1385
Longo, G., Capaccioli, M., & Ceriello, A. 1991, A&AS, 90, 375
Macri, L. M., Huchra, J. P., Sakai, S., Mould, J. R., & Hughes, S. M. G. 2000, ApJS, 128, 461
Makarova, L. 1999, A&AS, 139, 491
Mannucci, F., Basile, F., Poggianti, B. M., Cimatti, A., Daddi, E., Pozzetti, L., & Vanzi, L. 2001, MNRAS, 326, 745
Marcum, P. M., et al. 2001, ApJS, 132, 129
McCall, M. L. 1981, MNRAS, 194, 485
———. 1982, Publ. Univ. Texas Astron. Dept., No. 20 (Austin: Univ. Texas, Austin), 1
———. 1989, AJ, 97, 1341
McCall, M. L., & Armour, M.-H. 2000, in ASP Conf. Ser. 218, Mapping the Hidden Universe: The Universe Behind the Milky Way—The Universe in HI, ed. R. C. Kraan-Korteweg, P. A. Henning, & H. Andernach (San Francisco: ASP), 1
McCall, M. L., Rybski, P. M., & Shields, G. A. 1985, ApJS, 57, 1
Newman, J. A., Ferrarese, L., Stetson, P. B., Maoz, E., Zepf, S. E., Davis, M., Freedman, W. L., & Madore, B. F. 2001, ApJ, 553, 562
Nugent, P., Kim, A., & Perlmutter, S. 2002, PASP, 114, 803
O'Donnell, J. E. 1994, ApJ, 422, 158
Oke, J. B., Bertola, F., & Capaccioli, M. 1981, ApJ, 243, 453
Oke, J. B., & Gunn, J. E. 1983, ApJ, 266, 713
Olson, B. I. 1975, PASP, 87, 349
Paturel, G. 2004, Lyon-Meudon Extragalactic Database (LEDA) (Lyon: Obs. Lyon), http://leda.univ-lyon1.fr
Pickles, A. J. 1985, ApJ, 296, 340
———. 1998, PASP, 110, 863
Poggianti, B. M. 1997, A&AS, 122, 399
Racine, R. 1973, AJ, 78, 180
Riess, A. G., et al. 2004, ApJ, 607, 665
Rifatto, A., Longo, G., & Capaccioli, M. 1995a, A&AS, 109, 341
———. 1995b, A&AS, 114, 527
Schlegel, D. J., Finkbeiner, D. P., & Davis, M. 1998, ApJ, 500, 525
Schmidt, K. H. 1956, Mitt. Univ. Sternwarte Jena, No. 27
Schmidt-Kaler, Th. 1982, in Landolt-Bornstein New Series, Group VI, Vol. 2b, ed. K. Shaifers & H.-H. Voigt (Berlin: Springer), 12
Sloan Digital Sky Survey. 2004, Data Release 2 (Batavia, IL: Fermi Natl. Accelerator Lab.), http://www.sdss.org/DR2/instruments/imager/index.html#filters, http://www.sdss.org/DR2/algorithms/fluxcal.html
Shostak, G. S. 1978, A&A, 68, 321
Staveley-Smith, L., Davies, R. D., & Kinman, T. D. 1992, MNRAS, 258, 334
Swaters, R. A., & Balcells, M. 2002, A&A, 390, 863
Thuan, T. X., & Gunn, J. E. 1976, PASP, 88, 543
Tully, R. B., & Fouqué, P. 1985, ApJS, 58, 67
Tully, R. B., Pierce, M. J., Huang, J.-S., Saunders, W., Verheijen, M. A. W., & Witchalls, P. L. 1998, AJ, 115, 2264
Warmels, R. H. 1988, A&AS, 73, 453
Woudt, P. A., & Kraan-Korteweg, R. C. 2000, in ASP Conf. Ser. 218, Mapping the Hidden Universe: The Universe Behind the Milky Way—The Universe in HI, ed. R. C. Kraan-Korteweg, P. A. Henning, & H. Andernach (San Francisco: ASP), 193